Numerical schemes for the simulation of Inertial Confinement Fusion in the direct drive context

Pierre-Henri Maire, maire@celia.u-bordeaux1.fr

UMR CELIA, CNRS, University Bordeaux 1, CEA,
351, cours de la Libération, 33405 Talence, France
Collaborations: Rémi Abgrall, Jérôme Breil, Stéphane Galera, Guy Schurtz

Outline

- Context of Inertial Confinement Fusion
- Physical models
- Hydrodynamics code
- A cell-centered Lagrangian scheme
- Arbitrary Lagrangian Eulerian scheme
- Conclusions and perspectives

CELIA Laboratory (Bordeaux)

- In 2003, new French policy for lasers and plasmas
- Open CEA's facilities LIL and LMJ to academic users both national and European
  - Demonstrate fusion ignition in laboratory
  - Do basic science research: high energy density physics, astrophysics, hydrodynamics, plasma physics
- Create CELIA laboratory at University Bordeaux I
  - Parent bodies: CEA, CNRS and University Bordeaux I
  - 60 researchers, professors, docs and post-docs
  - Main topics: theoretical and experimental studies in the domain of laser plasma interaction and Inertial Confinement Fusion (Direct Drive)
- Need for CELIA laboratory of a 2D ICF code to prepare and reproduce the experiments on laser created plasmas

Context of ICF

- Controlled fusion to produce energy [Lindl, *Inertial Confinement Fusion*, Springer (1998)]

$$\mathrm{D} + \mathrm{T} \longrightarrow {}^4\mathrm{He} \quad (3.5\mathrm{MeV}) + \mathrm{n} \quad (14.1\mathrm{MeV})$$

- Two conditions to obtain fusion

  Temperature $T_i > T_{\mathrm{ign}},$ typical value $T_i \approx 60\ 10^6\ \mathrm{K}$

  Confinement $N\tau > 10^{14}\,\mathrm{cm}^{-3}\mathrm{s},$ Lawson criterion.

- Two approaches to fusion applicable to energy production

  Magnetic Confinement Fusion $\tau \approx 1\,\mathrm{s}, N \approx 10^{14}\,\mathrm{cm}^{-3}.$

  Inertial Confinement Fusion $\tau \approx 10^{-11}\,\mathrm{s}, N \approx 10^{25}\,\mathrm{cm}^{-3}.$

- Main facilities: International Thermonuclear Experimental Reactor, Laser Mega Joule, National Ignition Facility

Context of ICF

- View of the LMJ and LIL facilities (CEA CESTA near Bordeaux)

Context of ICF

- View of the LMJ laser bays

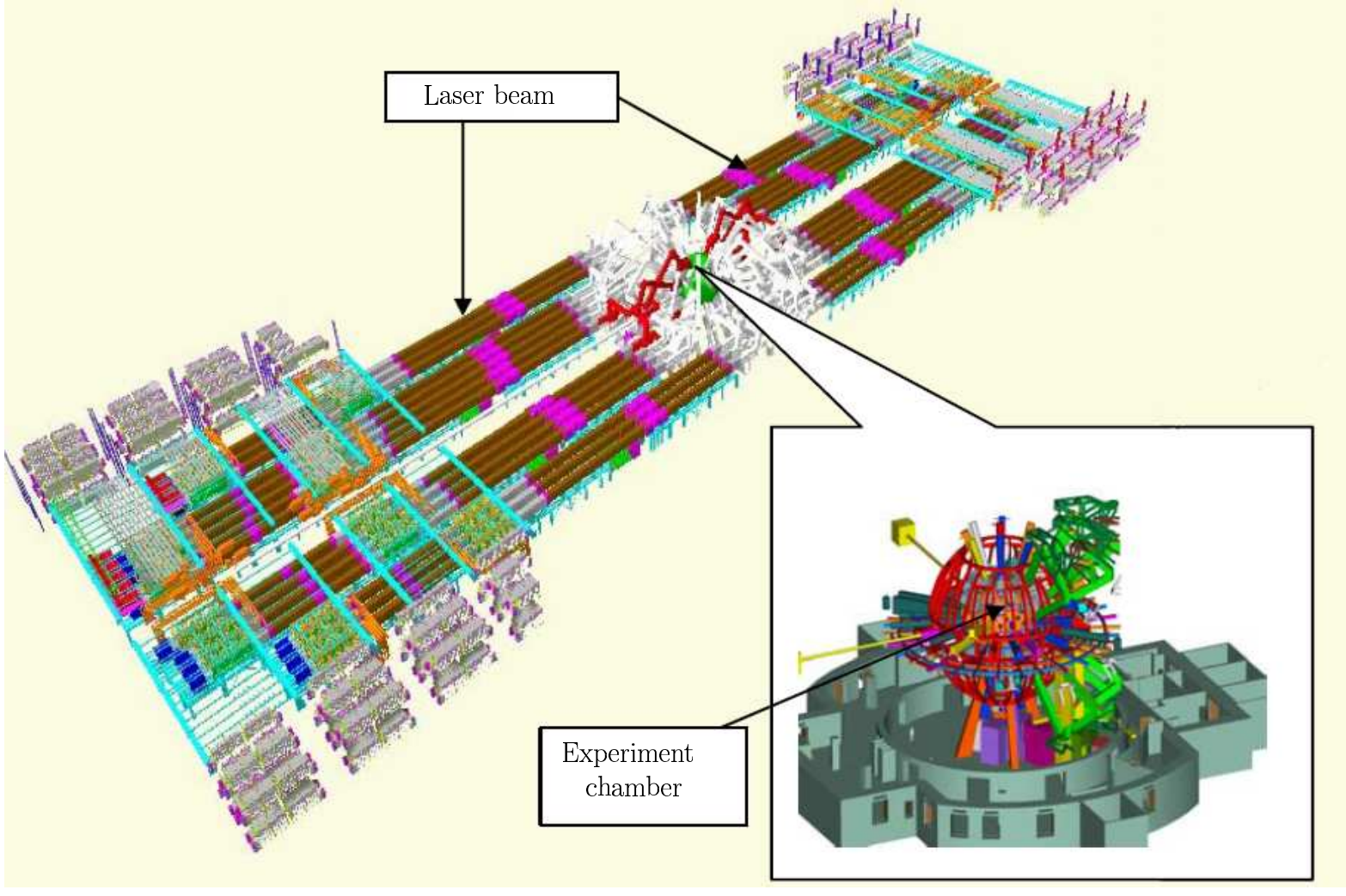

Context of ICF

- Picture of a target

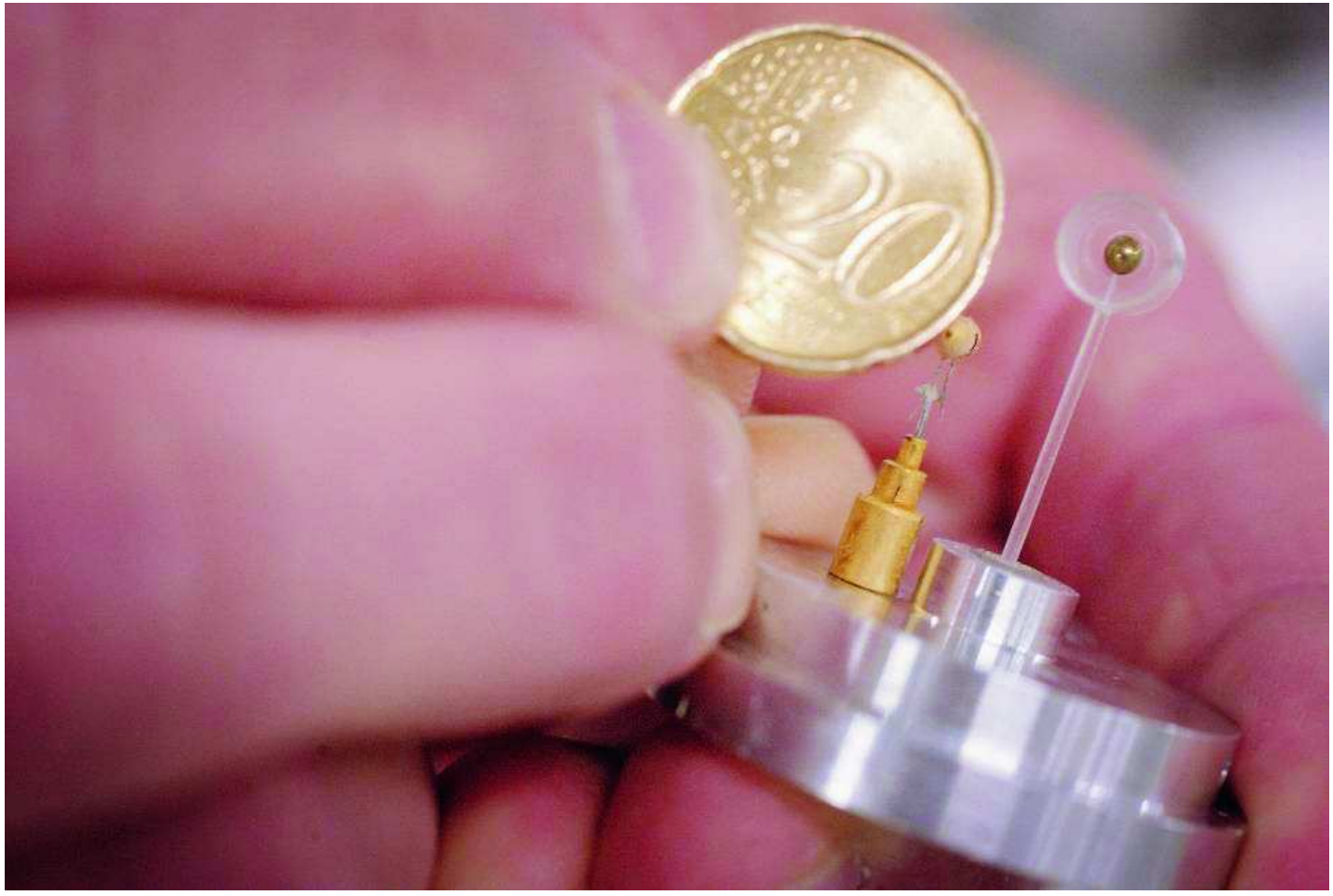

Context of ICF

- Two classical schemes for ICF

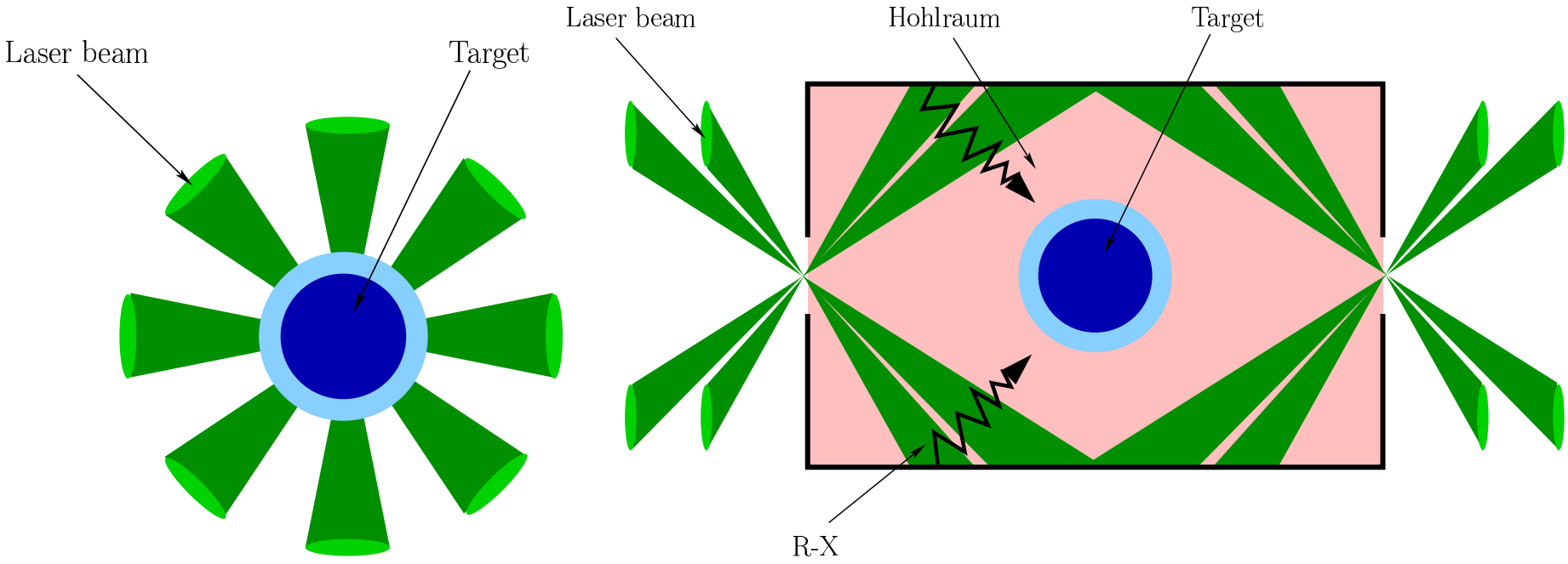

Direct Drive

Indirect Drive

Direct drive has a higher laser-target coupling efficiency but is less uniform in laser irradiation due to discrete beams of lasers.
The indirect drive, by soft X rays which are generated at the inner surface of the holraum, can have a higher uniform irradiation to reduce the growth of perturbations due to Rayleigh-Taylor (RT) instabilities.

Phenomenology of Direct Drive ICF

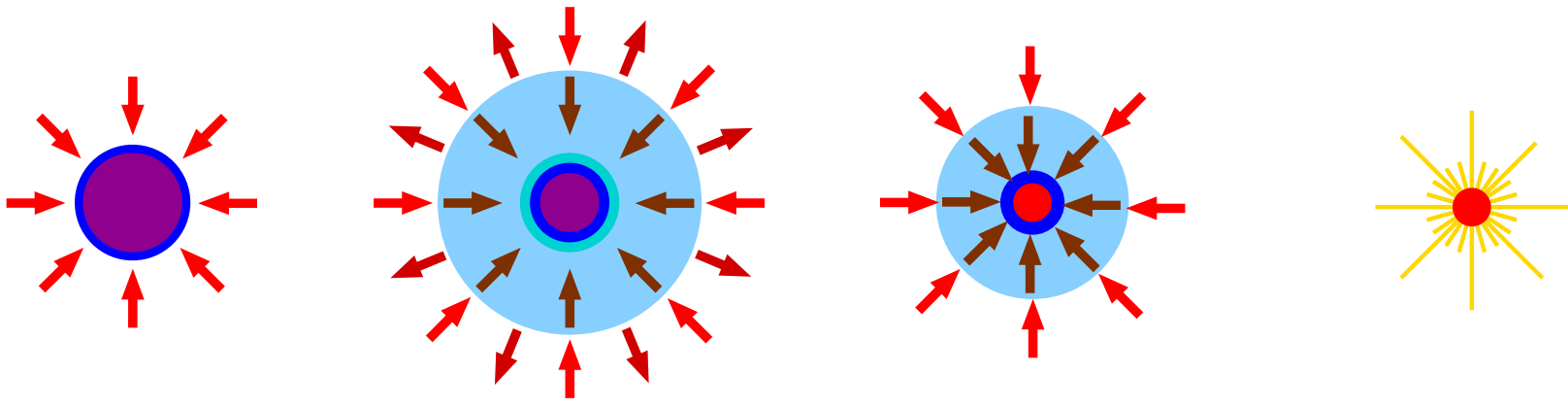

Laser heating DT compression Hot spot ignition Thermonuclear burn

Main issues for Direct Drive ICF

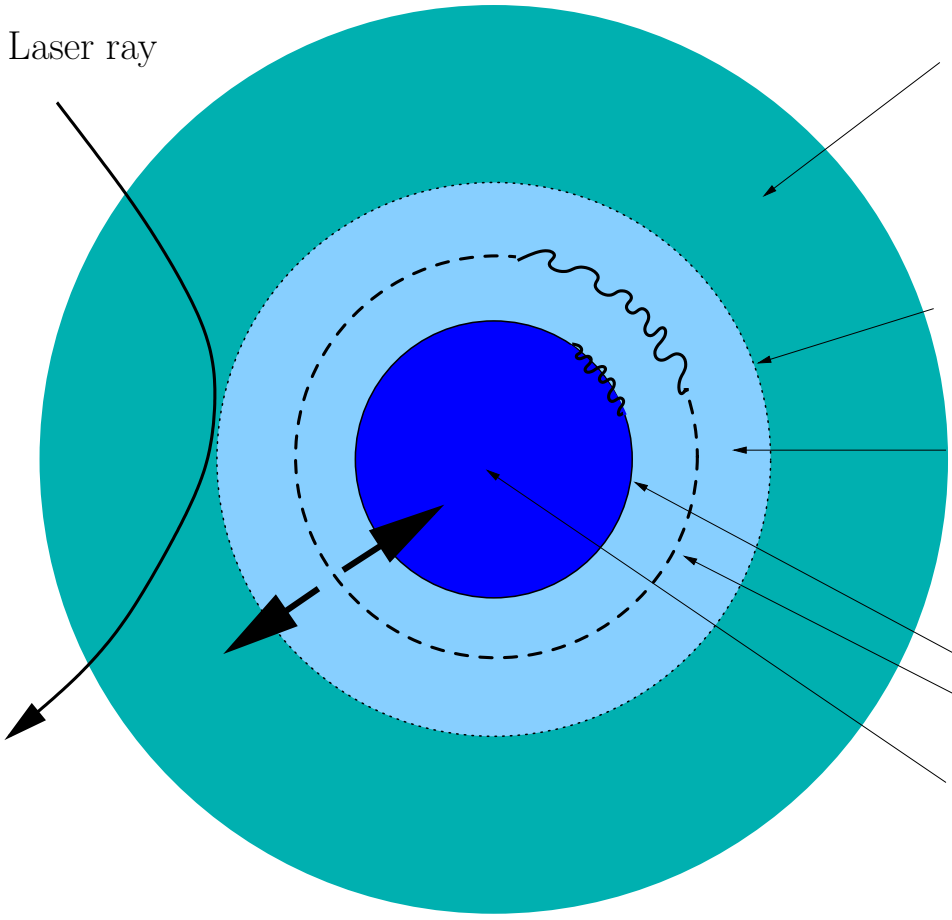

CORONA

Energy absorption
Laser plasma interaction

CRITICAL SURFACE

CONDUCTION ZONE

Electron heat transport
Ablation

HYDRODYNAMIC INSTABILITIES

Interface
Ablation front

COMPRESSED FUEL

Ignition
Thermonuclear combustion
Charged particles transport

Target design for Direct Drive ICF

- HiPER Project [www.hiper-laser.org]

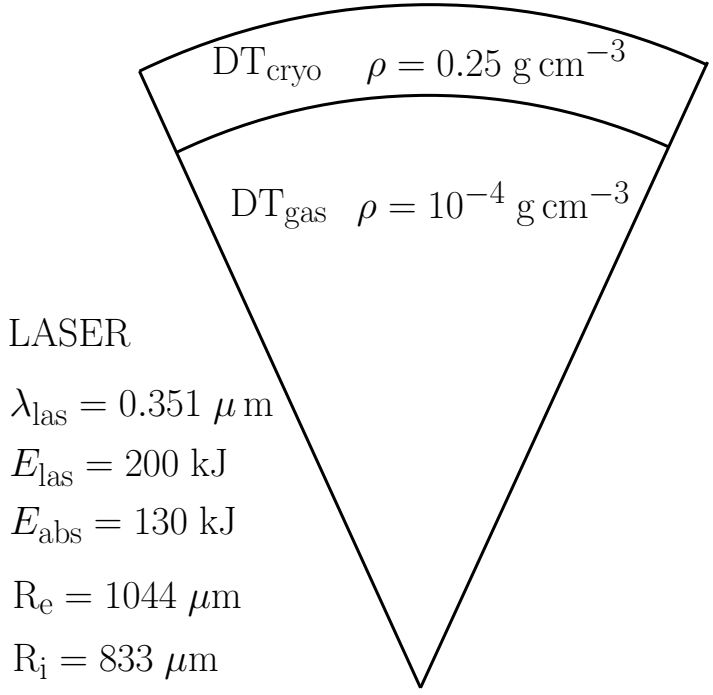

All DT target

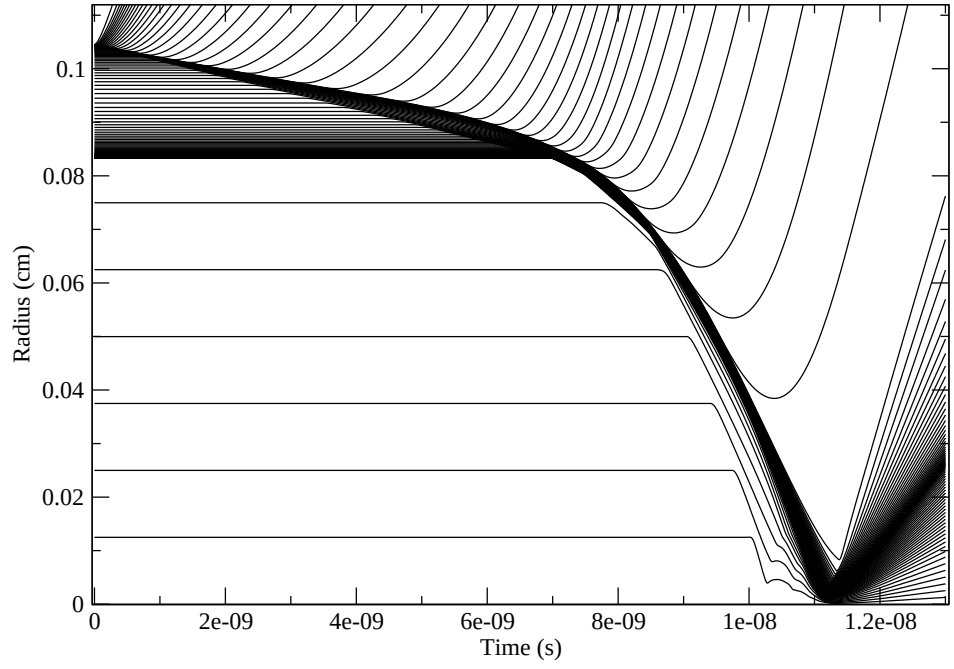

R-t diagram

Target design for Direct Drive ICF

- HiPER Project

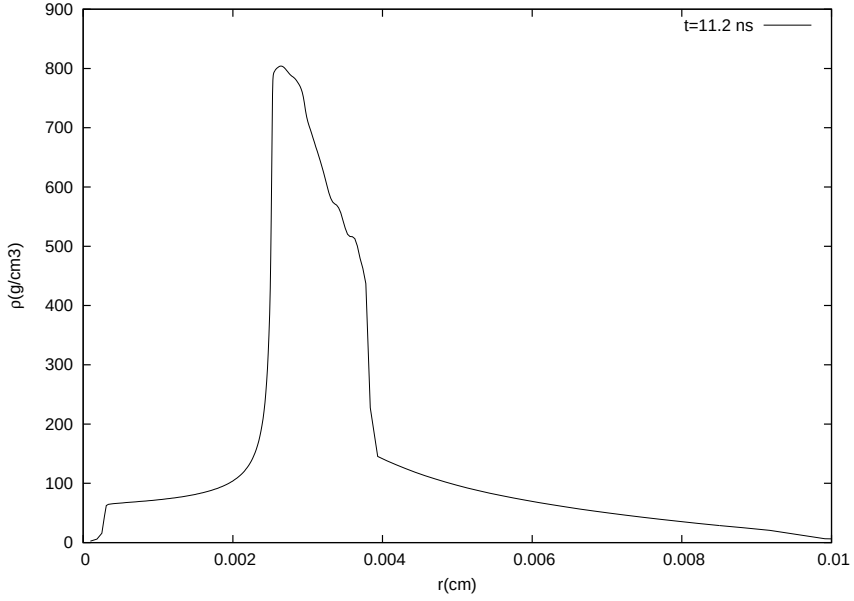

Density profile at stagnation

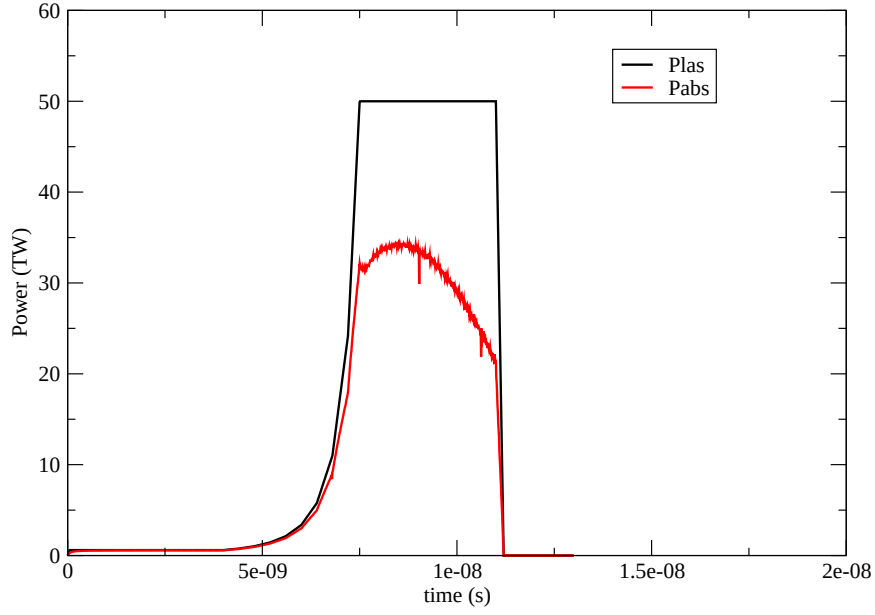

Pulse shaping

Compression rates $\sim 10^5$ in $\mathrm{DT}_{\mathrm{gas}}$ and $\sim 10^3$ in $\mathrm{DT}_{\mathrm{cryo}}$. Pulse shaping in order to obtain the highest compression rate by minimizing entropy deposition.

Motivations for a Lagrangian formulation

- ICF plasma is created by laser interaction with target
- ICF target is the assembly of multimaterial layers with high aspect ratios
- Multimaterial flows with large displacements, strong shocks and rarefaction waves
- Simulations with large changes of computational domain volume and shape (animation)
- Lagrangian formulation is well adapted to ICF flows
  - Mesh moves with the fluid
  - Shock resolution is increased
  - No mass flux between cell
  - Free surfaces are naturaly treated
  - Interfaces are sharply resolved
- However for too large deformations (shear and vorticity) it appears a lack of robustness (tangled mesh)
- It can be treated by using an Arbitrary Lagrangian Eulerian (ALE) strategy

Physical model

- Plasma fluid model in Lagrangian formalism

$$\rho\frac{d\tau}{dt} - \nabla\cdot\boldsymbol{V} = 0,$$

$$\rho\frac{d\boldsymbol{V}}{dt} + \boldsymbol{\nabla}(P_{\mathrm{i}} + P_{\mathrm{e}}) = \boldsymbol{0},$$

$$\rho\left(\frac{d\varepsilon_{\mathrm{e}}}{dt} + P_{\mathrm{e}}\frac{d\tau}{dt}\right) - \nabla\cdot(\lambda_{\mathrm{e}}\boldsymbol{\nabla}T_{\mathrm{e}}) = \Omega_{\mathrm{ei}}(T_{\mathrm{i}} - T_{\mathrm{e}}) + W_{\mathrm{las}} + W_{\mathrm{rad}} + W^{\mathrm{e}}_{\mathrm{fus}} + \nabla\cdot\boldsymbol{Q}^{\mathbf{nl}}_{\mathbf{e}},$$

$$\rho\left(\frac{d\varepsilon_{\mathrm{i}}}{dt} + P_{\mathrm{i}}\frac{d\tau}{dt}\right) - \nabla\cdot(\lambda_{\mathrm{i}}\boldsymbol{\nabla}T_{\mathrm{i}}) = \Omega_{\mathrm{ei}}(T_{\mathrm{e}} - T_{\mathrm{i}}) + W^{\mathrm{i}}_{\mathrm{fus}},$$

$$\frac{\partial\boldsymbol{B}}{\partial t} = \boldsymbol{\nabla}\times\left[\boldsymbol{V}\times\boldsymbol{B} + \frac{c}{eN_{\mathrm{e}}}\boldsymbol{\nabla}\left(N_{\mathrm{e}}T_{\mathrm{e}}\right) + \frac{c}{e}\beta\cdot\boldsymbol{\nabla}T_{\mathrm{e}} - \frac{c^2}{4\pi}\sigma\cdot\boldsymbol{\nabla}\times\boldsymbol{B}\right].$$

λ_e tensorial conductivity (Spitzer-Härm and Braginskii), β is the thermoelectric tensor and σ is the tensorial resistivity.
Tranverse MHD with magnetic pressure and Joule heating neglected.
$\boldsymbol{Q}^{\mathbf{nl}}_{\mathbf{e}}$ is the non local heat flux.

2D ICF code

- CHIC : 2D ICF code developped at CELIA

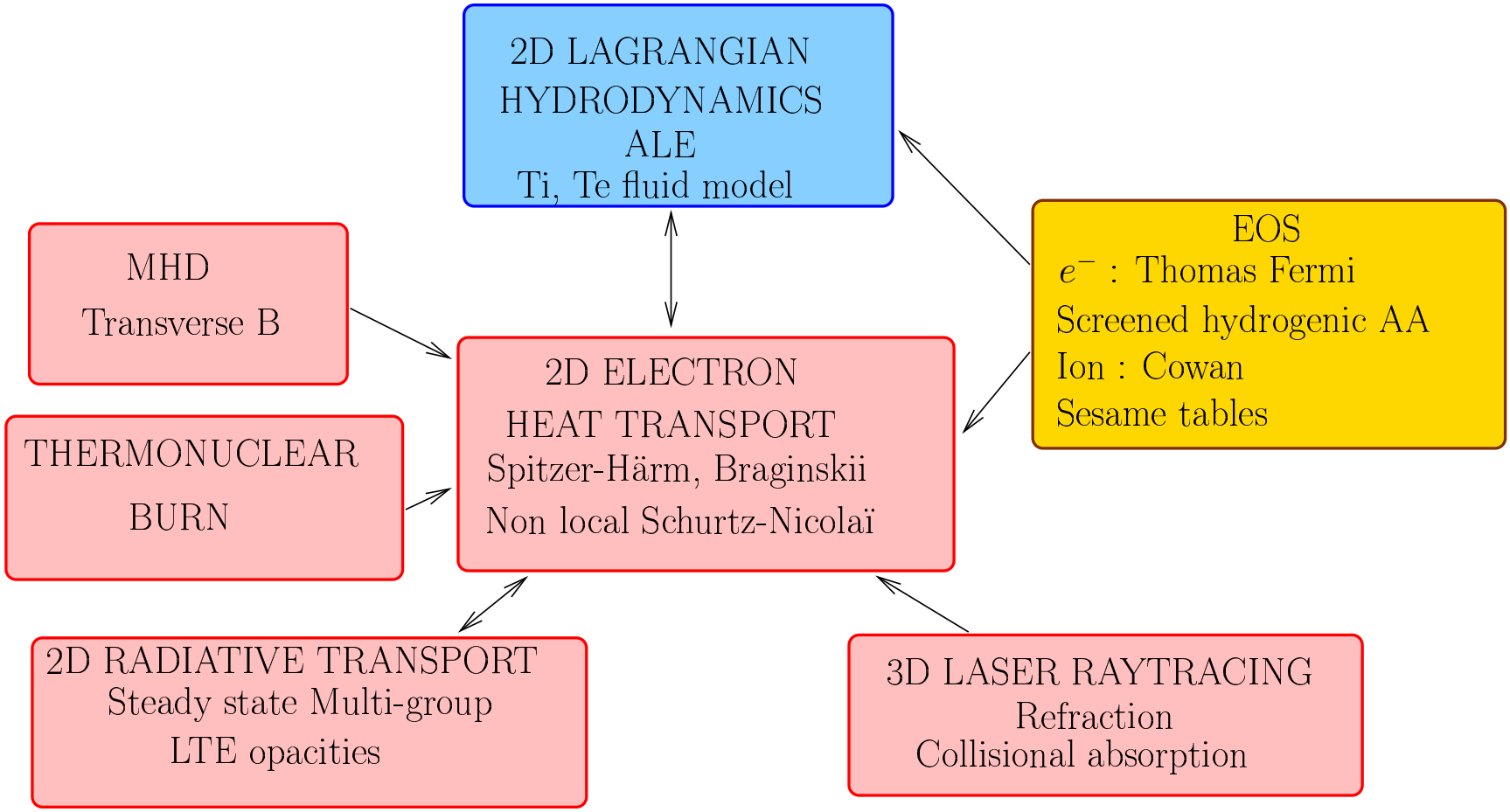

Review on 2D Lagrangian schemes

- Staggered schemes
  - Velocity at grid nodes
  - Internal energy formulation and artificial viscosity
  - Wilkins scheme [MCP **3**, (1964)]
  - Compatible discretization [Caramana and Shashkov JCP **146**, (1998)]
- Centered schemes
  - CAVEAT scheme [Dukowicz et al. Report LA-10613-MS, (1986)]
    - 2D conservative extension of Godunov scheme
    - Node velocity computed with a least squares procedure
    - Fluxes not consistent with the nodes motion
  - Després Mazeran scheme [ARMA **178**, (2005)]
    - Analysis of 2D gas dynamics in fully Lagrangian form
    - Conservative and entropy consistent 2D scheme
    - **Strong dependence to the cell aspect ratio**
    - Some problems with boundary conditions

Introduction and motivations

- Motivations
  - Develop a new cell-centered Lagrangian scheme
  - Cell-centered momentum is easier to handle in view of ALE extension
- Main features of our scheme
  - Four pressures on each edge
  - 2D nodal solver
  - Conservative and entropy consistent
  - Recovers the classical Godunov acoustic solver for 1D flows
  - First order accurate
  - Second order extension

R. Abgrall, J. Breil, P.-H. Maire, J. Ovadia. A cell-centered Lagrangian scheme for two-dimensional compressible flow problems. *to appear in SIAM Journal of Scientific Computing* 2007; https://hal.inria.fr/inria-00113542.

Governing equations

- Lagrangian hydrodynamics

For a control volume $\Omega(t)$ moving with the fluid velocity $\boldsymbol{V} = (u, v)^t$

$$\frac{d}{dt}\int_{\Omega(t)} \rho \,\mathrm{d}\Omega = 0, \quad \text{mass conservation}$$

$$\frac{d}{dt}\int_{\Omega(t)} \mathrm{d}\Omega - \int_{\partial\Omega(t)} \boldsymbol{V}\cdot\boldsymbol{N}\,\mathrm{d}l = 0, \quad \text{volume conservation}$$

$$\frac{d}{dt}\int_{\Omega(t)} \rho\boldsymbol{V}\,\mathrm{d}\Omega + \int_{\partial\Omega(t)} P\boldsymbol{N}\,\mathrm{d}l = \boldsymbol{0}, \quad \text{momentum conservation}$$

$$\frac{d}{dt}\int_{\Omega(t)} \rho E\,\mathrm{d}\Omega + \int_{\partial\Omega(t)} P\boldsymbol{V}\cdot\boldsymbol{N}\,\mathrm{d}l = 0. \quad \text{total energy conservation}$$

The pressure P is given by the equation of state $P \equiv P(\rho, \varepsilon)$ where $\varepsilon = E - \frac{1}{2}\boldsymbol{V}\cdot\boldsymbol{V}$.
Note that the volume conservation equation is also a geometrical law conservation.

Spatial discretization

- Discrete evolution equations for $(\tau_c = 1/\rho_c, \boldsymbol{V_c}, E_c)$

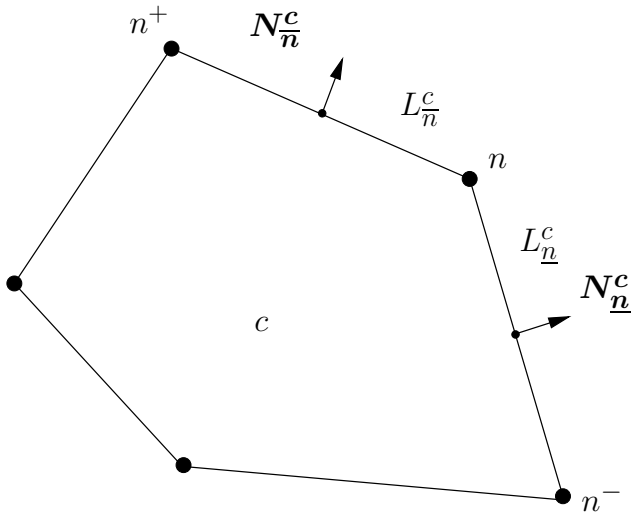

$$L^c_{\underline{n}} = \mathrm{d}(n, (n+n^-)/2),$$
$$L^c_{\overline{n}} = \mathrm{d}(n, (n+n^+)/2).$$

$$\frac{d}{dt} m_c = 0,$$
$$m_c \frac{d}{dt} \tau_c - \int_{\partial c} \boldsymbol{V} \cdot \boldsymbol{N} \, \mathrm{d}l = 0,$$
$$m_c \frac{d}{dt} \boldsymbol{V_c} + \int_{\partial c} P\boldsymbol{N} \, \mathrm{d}l = \boldsymbol{0},$$
$$m_c \frac{d}{dt} E_c + \int_{\partial c} P\boldsymbol{V} \cdot \boldsymbol{N} \, \mathrm{d}l = 0.$$

Trajectories equation : $\dfrac{d}{dt}\boldsymbol{X_n} = \boldsymbol{V_n^\star}, \ \boldsymbol{X_n}(0) = \boldsymbol{x_n}(0).$

Note that the cell area satisfies $A_c = m_c \tau_c$.

Spatial discretization

- Nodal approximation of the geometrical law conservation

Compute the area of the cell using a triangular decomposition

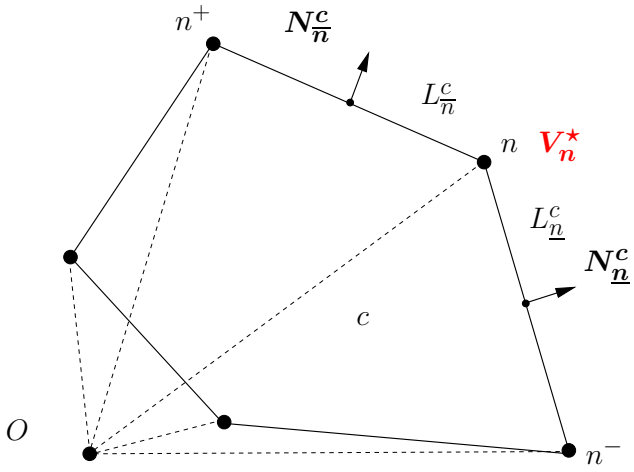

$$A_c = \frac{1}{2} \sum_{n \in \mathcal{N}(c)} (\boldsymbol{On} \times \boldsymbol{On}_+) \cdot \boldsymbol{e_Z},$$

time differentiation leads to

$$\frac{d}{dt} A_c = \sum_{n \in \mathcal{N}(c)} \left(L^c_{\underline{n}} \boldsymbol{N}^{\boldsymbol{c}}_{\boldsymbol{\underline{n}}} + L^c_{\overline{n}} \boldsymbol{N}^{\boldsymbol{c}}_{\boldsymbol{\overline{n}}} \right) \cdot \boldsymbol{V}^{\star}_{\boldsymbol{n}},$$

where $\mathcal{N}(c)$ is the set of vertices of cell c.

We need to compute first the nodal velocity in order to satisfy the geometrical law conservation. This is the only way to ensure the compatibility between vertex motion and cell area variation.

Spatial discretization

- Nodal approximation of the momentum flux

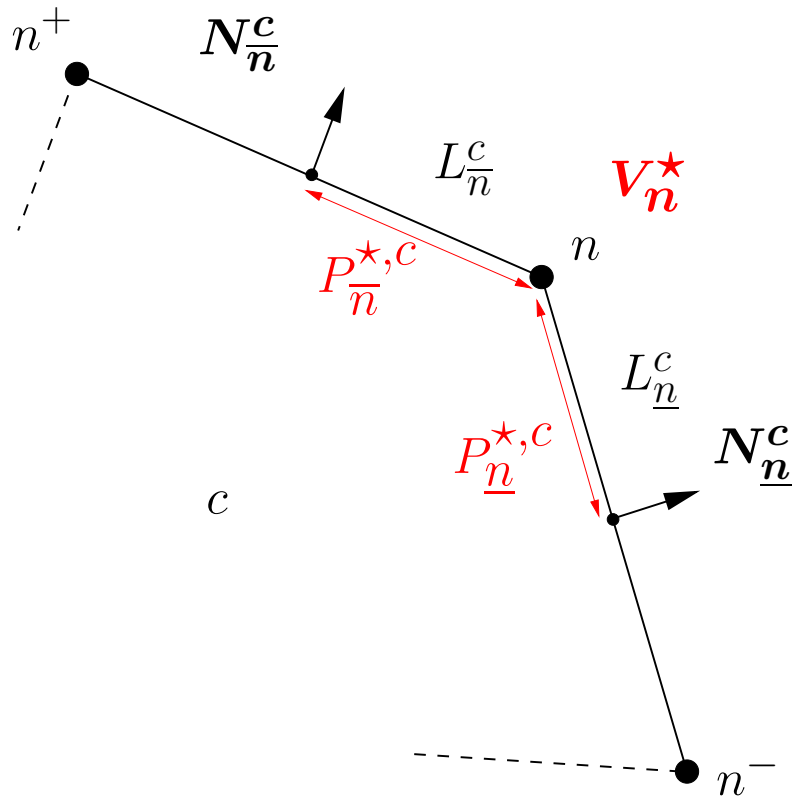

$P_{\underline{n}}^{\star,c}$ and $P_{\overline{n}}^{\star,c}$ pressures on both sides of node n, viewed from cell c.

The momentum equation is written

$$m_c \frac{d}{dt}\boldsymbol{V_c} + \sum_{n\in\mathcal{N}(c)} \left(L_{\underline{n}}^c P_{\underline{n}}^{\star,c} \boldsymbol{N_{\underline{n}}^c} + L_{\overline{n}}^c P_{\overline{n}}^{\star,c} \boldsymbol{N_{\overline{n}}^c} \right) = \mathbf{0}.$$

Spatial discretization

- Evolution equations for the discrete unknowns $(\tau_c, \boldsymbol{V_c}, E_c)$

$$m_c \frac{d}{dt}\tau_c - \sum_{n\in\mathcal{N}(c)} \left(L_{\underline{n}}^{c} \boldsymbol{N}_{\underline{\boldsymbol{n}}}^{\boldsymbol{c}} + L_{\overline{n}}^{c} \boldsymbol{N}_{\overline{\boldsymbol{n}}}^{\boldsymbol{c}} \right) \cdot \boldsymbol{V}_{\boldsymbol{n}}^{\star} = 0,$$

$$m_c \frac{d}{dt}\boldsymbol{V_c} + \sum_{n\in\mathcal{N}(c)} \left(L_{\underline{n}}^{c} P_{\underline{n}}^{\star,c} \boldsymbol{N}_{\underline{\boldsymbol{n}}}^{\boldsymbol{c}} + L_{\overline{n}}^{c} P_{\overline{n}}^{\star,c} \boldsymbol{N}_{\overline{\boldsymbol{n}}}^{\boldsymbol{c}} \right) = \boldsymbol{0},$$

$$m_c \frac{d}{dt}E_c + \sum_{n\in\mathcal{N}(c)} \left(L_{\underline{n}}^{c} P_{\underline{n}}^{\star,c} \boldsymbol{N}_{\underline{\boldsymbol{n}}}^{\boldsymbol{c}} + L_{\overline{n}}^{c} P_{\overline{n}}^{\star,c} \boldsymbol{N}_{\overline{\boldsymbol{n}}}^{\boldsymbol{c}} \right) \cdot \boldsymbol{V}_{\boldsymbol{n}}^{\star} = 0.$$

- Node motion $$\frac{d}{dt}\boldsymbol{X_n} = \boldsymbol{V}_{\boldsymbol{n}}^{\star}, \quad \boldsymbol{X_n}(0) = \boldsymbol{x_n}.$$

Construction of a nodal solver to evaluate the nodal fluxes $\boldsymbol{V}_{\boldsymbol{n}}^{\star}$, $P_{\underline{n}}^{\star,c}$ and $P_{\overline{n}}^{\star,c}$.

Spatial discretization

- Remark1 : momentum flux approximation

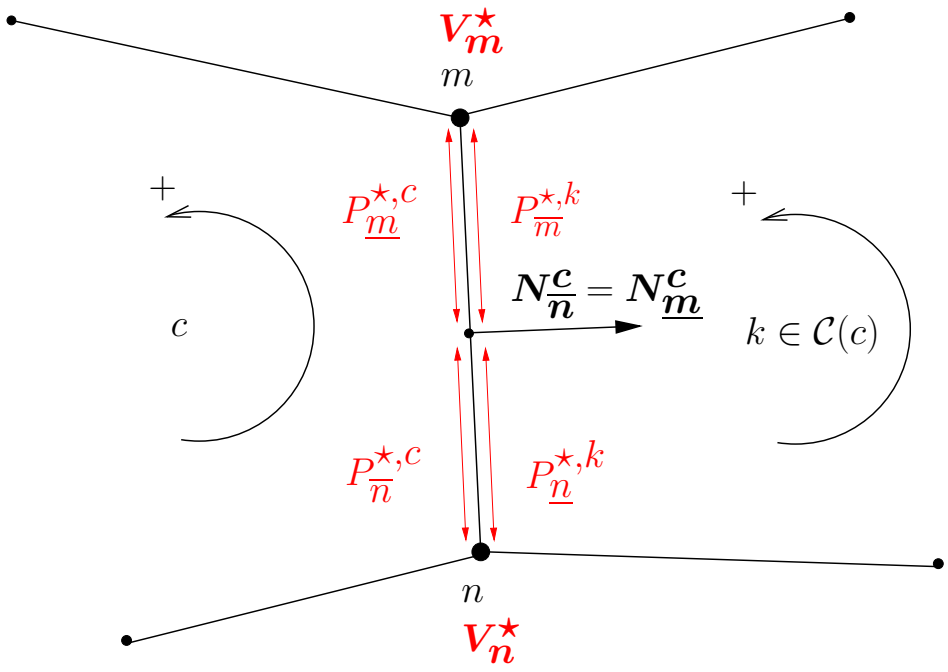

2 pressures on $[n, m]$ from cell c
2 pressures on $[n, m]$ from cell k

Generally, $P_{\overline{n}}^{\star,c} \neq P_{\underline{n}}^{\star,k}$ and $P_{\underline{m}}^{\star,c} \neq P_{\overline{m}}^{\star,k}$.

Contrarily to 1D Riemann solver approach momentum conservation is not ensured automatically! But we shall show how to recover it.

Spatial discretization

- Remark2 : local entropy inequality

Starting from Gibbs relation $T\mathrm{d}S = \mathrm{d}\varepsilon + P\mathrm{d}\tau$, we get

$$m_c\left(\frac{d\varepsilon_c}{dt} + P_c\frac{d\tau_c}{dt}\right) = \sum_{n\in\mathcal{N}(c)}\left[L^c_{\underline{n}}(P_c - P^{\star,c}_{\underline{n}})\boldsymbol{N^c_{\underline{n}}} + L^c_{\overline{n}}(P_c - P^{\star,c}_{\overline{n}})\boldsymbol{N^c_{\overline{n}}}\right]\cdot(\boldsymbol{V^\star_n} - \boldsymbol{V_c})$$

A sufficient condition to have an entropy inequality is to set

$$P_c - P^{\star,c}_{\underline{n}} = Z_c\,(\boldsymbol{V^\star_n} - \boldsymbol{V_c})\cdot\boldsymbol{N^c_{\underline{n}}},$$
$$P_c - P^{\star,c}_{\overline{n}} = Z_c\,(\boldsymbol{V^\star_n} - \boldsymbol{V_c})\cdot\boldsymbol{N^c_{\overline{n}}},$$

where $Z_c > 0$ is the acoustic impedance of the cell c.
We recover Riemann invariants along directions $\boldsymbol{N^c_{\underline{n}}}$ and $\boldsymbol{N^c_{\overline{n}}}$.

$$m_c T_c\frac{dS_c}{dt} = \sum_{n\in\mathcal{N}(c)} Z_c\left\{L^c_{\underline{n}}[(\boldsymbol{V^\star_n} - \boldsymbol{V_c})\cdot\boldsymbol{N^c_{\underline{n}}}]^2 + L^c_{\overline{n}}[(\boldsymbol{V^\star_n} - \boldsymbol{V_c})\cdot\boldsymbol{N^c_{\overline{n}}}]^2\right\} \geq 0.$$

Nodal solver

- Weighted least squares procedure for the vertex velocity

$\boldsymbol{V_n^\star} = (u_n^\star, v_n^\star)^t$ minimizes the functional

$$I(u_n^\star, v_n^\star) = \sum_{c^-,c} \omega_{c^-,c} \left(\boldsymbol{V_n^\star} \cdot \boldsymbol{N_{c^-,c}} - \mathcal{V}_{c^-,c}^\star \right)^2 .$$

$\boldsymbol{N_{c^-,c}} = \boldsymbol{N_{\underline{n}}^{c^-}} = -\boldsymbol{N_{\underline{n}}^{c}}$

$\omega_{c^-,c}$ weight on edge $[c^-, c]$

$\mathcal{V}_{c^-,c}^\star$ normal Riemann velocity on $[c^-, c]$

$$\mathcal{V}_{c^-,c}^\star = \left(\frac{Z_c \boldsymbol{V_c} + Z_{c^-} \boldsymbol{V_{c^-}}}{Z_c + Z_{c^-}} \right) \cdot \boldsymbol{N_{c^-,c}} - \frac{P_c - P_{c^-}}{Z_c + Z_{c^-}}$$

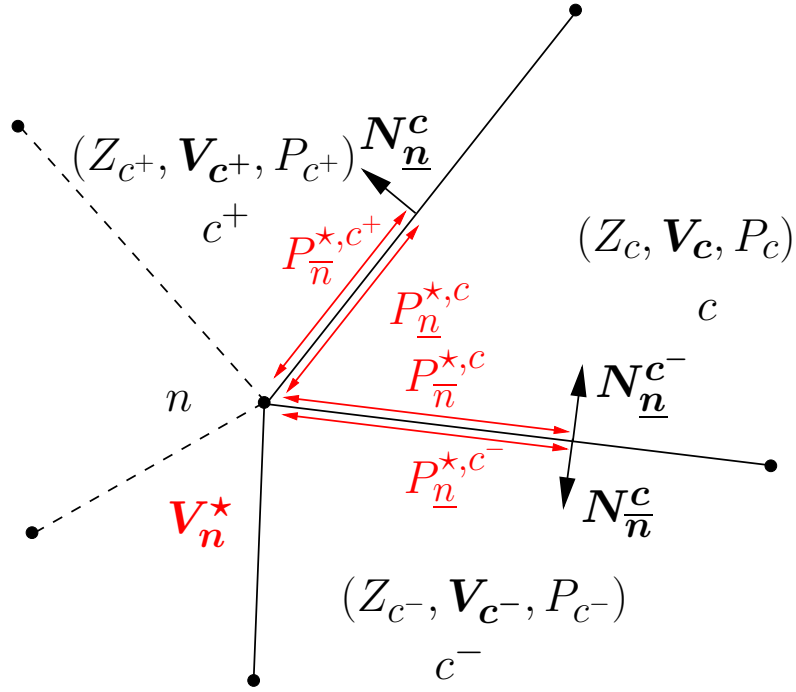

$\omega_{c^-,c}$ **will be computed so that momentum conservation will be recovered.**

Nodal solver

- Weights evaluation

Least squares problem posed by $\boldsymbol{\nabla} I = \mathbf{0}$, this yields the vectorial equation

$$\sum_{c^-,c} \omega_{c^-,c} \left(\boldsymbol{V_n^\star} \cdot \boldsymbol{N_{c^-,c}} - \mathcal{V}^\star_{c^-,c} \right) \boldsymbol{N_{c^-,c}} = \mathbf{0}. \tag{1}$$

Riemann invariants

$$P_{c^-} - P^{\star,c^-}_{\underline{n}} = Z_{c^-} \left(\boldsymbol{V_n^\star} - \boldsymbol{V_{c^-}} \right) \cdot \boldsymbol{N_{c^-,c}},$$
$$P_c - P^{\star,c}_{\overline{n}} = -Z_c \left(\boldsymbol{V_n^\star} - \boldsymbol{V_c} \right) \cdot \boldsymbol{N_{c^-,c}}.$$

By substraction of the Riemann invariants

$$P^{\star,c}_{\overline{n}} - P^{\star,c^-}_{\underline{n}} = (Z_c + Z_{c^-}) \left(\boldsymbol{V_n^\star} \cdot \boldsymbol{N_{c^-,c}} - \mathcal{V}^\star_{c^-,c} \right). \tag{2}$$

Since $\boldsymbol{V_n^\star} \cdot \boldsymbol{N_{c^-,c}} \neq \mathcal{V}^\star_{c^-,c}$ then $P^{\star,c}_{\overline{n}} \neq P^{\star,c^-}_{\underline{n}}$ (momentum conservation loss).

Nodal solver

- Weights evaluation

Substituting (2) in (1)

$$\sum_{c^-,c} \frac{\omega_{c^-,c}}{Z_c + Z_{c^-}} \left(P_{\overline{n}}^{\star,c} - P_{\underline{n}}^{\star,c^-} \right) \boldsymbol{N}_{\boldsymbol{c^-,c}} = \mathbf{0}. \tag{3}$$

It can be interpretated as a momentum balance around node n provided

$$\boxed{\omega_{c^-,c} = L_{c^-,c} \left(Z_c + Z_{c^-} \right),}$$

where $L_{c^-,c} = L_{\overline{n}}^{c} = L_{\underline{n}}^{c^-}$.

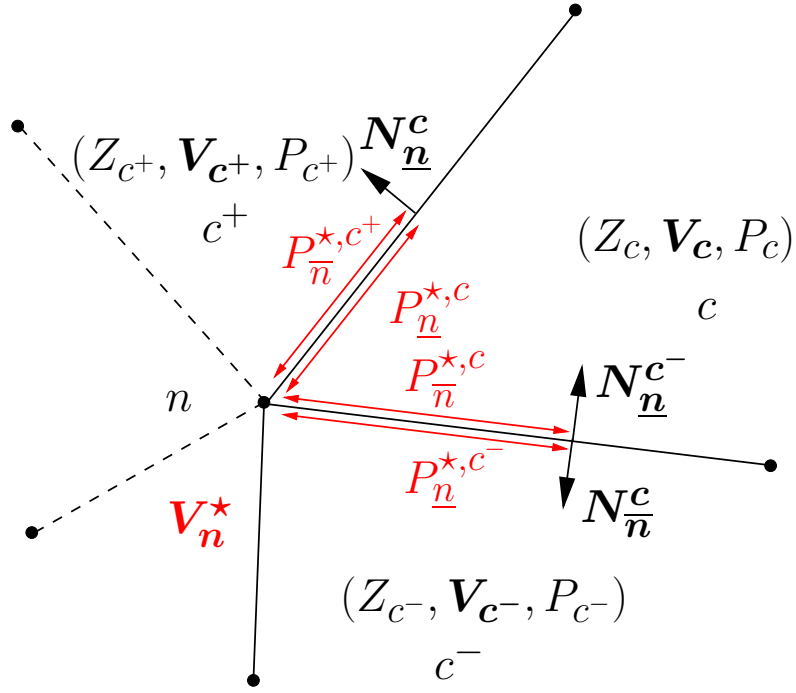

Nodal solver

- Momentum and energy conservation

With these weights one can check that

$$\sum_{c \in \mathcal{C}(n)} \left(L_{\underline{n}}^{c} P_{\underline{n}}^{\star,c} \boldsymbol{N}_{\underline{\boldsymbol{n}}}^{\boldsymbol{c}} + L_{\overline{n}}^{c} P_{\overline{n}}^{\star,c} \boldsymbol{N}_{\overline{\boldsymbol{n}}}^{\boldsymbol{c}} \right) = \mathbf{0},$$

$$\sum_{c \in \mathcal{C}(n)} \left(L_{\underline{n}}^{c} P_{\underline{n}}^{\star,c} \boldsymbol{N}_{\underline{\boldsymbol{n}}}^{\boldsymbol{c}} + L_{\overline{n}}^{c} P_{\overline{n}}^{\star,c} \boldsymbol{N}_{\overline{\boldsymbol{n}}}^{\boldsymbol{c}} \right) \cdot \boldsymbol{V}_{\boldsymbol{n}}^{\star} = \mathbf{0},$$

where $\mathcal{C}(n)$ is the set of the cells sharing node n.

We have recovered momentum and total energy conservation.

Nodal solver

- Summary of nodal fluxes computation

$$\boldsymbol{V}_{\boldsymbol{n}}^{\star} = \left(\sum_{c^-,c} \omega_{c^-,c} \boldsymbol{N}_{\boldsymbol{c^-,c}} \otimes \boldsymbol{N}_{\boldsymbol{c^-,c}} \right)^{-1} \left(\sum_{c^-,c} \omega_{c^-,c} \mathcal{V}_{c^-,c}^{\star} \boldsymbol{N}_{\boldsymbol{c^-,c}} \right),$$

$$P_{c^-} - P_{\underline{n}}^{\star,c^-} = Z_{c^-} \left(\boldsymbol{V}_{\boldsymbol{n}}^{\star} - \boldsymbol{V}_{\boldsymbol{c^-}} \right) \cdot \boldsymbol{N}_{\boldsymbol{c^-,c}},$$

$$P_c - P_{\overline{n}}^{\star,c} = -Z_c \left(\boldsymbol{V}_{\boldsymbol{n}}^{\star} - \boldsymbol{V}_{\boldsymbol{c}} \right) \cdot \boldsymbol{N}_{\boldsymbol{c^-,c}},$$

$$\mathcal{V}_{c^-,c}^{\star} = \left(\frac{Z_c \boldsymbol{V}_{\boldsymbol{c}} + Z_{c^-} \boldsymbol{V}_{\boldsymbol{c^-}}}{Z_c + Z_{c^-}} \right) \cdot \boldsymbol{N}_{\boldsymbol{c^-,c}} - \frac{P_c - P_{c^-}}{Z_c + Z_{c^-}},$$

$$\omega_{c^-,c} = L_{c^-,c} \left(Z_c + Z_{c^-} \right).$$

We can check that the nodal velocity is always defined provided the mesh is non-degenerate (Schwarz inequality).

Nodal solver

- 1D flow with planar symmetry

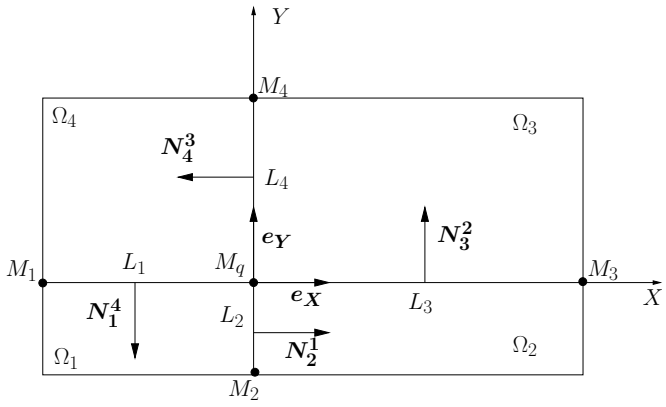

Cells 1 and 4: state P_1, Z_1, $\boldsymbol{V_1} = u_1 \boldsymbol{e_X}$.
Cells 2 and 3: state P_2, Z_2, $\boldsymbol{V_2} = u_2 \boldsymbol{e_X}$.

Simple calculations yields $A = (L_2 + L_4)(Z_1 + Z_2)$, $B = 2(L_1 Z_1 + L_3 Z_2)$, $C = 0$, $SM_X = (L_2 + L_4)(P_1 - P_2 + Z_1 u_1 + Z_2 u_2)$ and $SM_Y = 0$. Therefore, the nodal velocity is given by

$$u_q^\star = \frac{P_1 - P_2 + Z_1 u_1 + Z_2 u_2}{Z_1 + Z_2},$$
$$v_q^\star = 0.$$

We recover exactly the 1D Godunov acoustic solution!

Nodal solver

- 1D flow with cylindrical symmetry

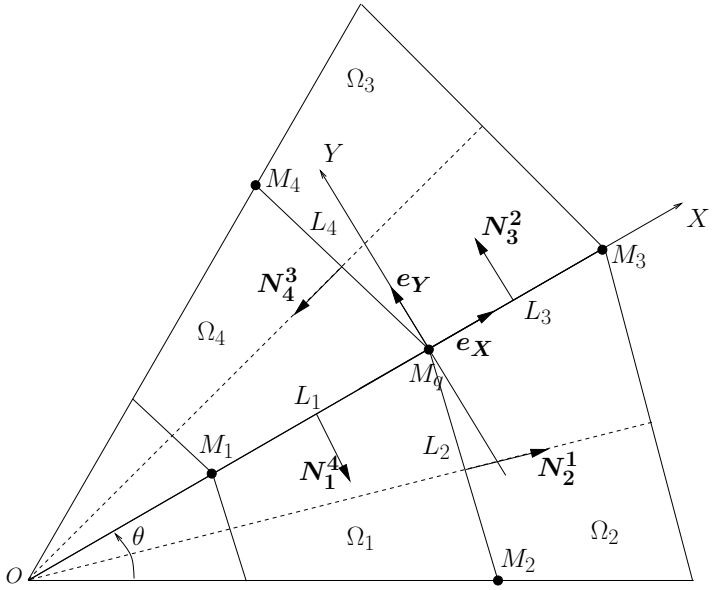

Consider an equi-angular polar mesh.
Choose the local frame $(M_q, \boldsymbol{e_X}, \boldsymbol{e_Y})$.
Cells 1 and 4: state P_1, Z_1, $\boldsymbol{V_1} = V_1 \boldsymbol{N_2^1}$, $\boldsymbol{V_4} = -V_1 \boldsymbol{N_4^3}$.
Cells 2 and 3: state P_2, Z_2, $\boldsymbol{V_2} = V_2 \boldsymbol{N_2^1}$, $\boldsymbol{V_3} = -V_2 \boldsymbol{N_4^3}$.

The cylindrical symmetry provides

$$u_q^\star = \frac{P_1 - P_2 + Z_1 V_1 + Z_2 V_2}{Z_1 + Z_2} \frac{1}{\cos(\frac{\theta}{2})},$$

$$v_q^\star = 0.$$

Once more the Godunov acoustic solver modified by a geometrical factor.

Spatial discretization

- Comments
  - Vertex velocity and fluxes computed consistently
  - Local entropy inequality
  - Momentum and total energy conservation
  - Naturally unstructured
  - Recover classical Godunov acoustic solver for 1D flows
  - Boundary conditions easily derived
  - Tabulated EOS provided the isentropic sound speed is known.
  - Spatial approximation first order accurate

Second order extension

- Piecewise linear reconstruction for P and $\boldsymbol{V}$ using P_c and $\boldsymbol{V_c}$

$$\phi_c(\boldsymbol{X}) = \phi(\boldsymbol{X_c}) + \boldsymbol{\nabla}\phi_c \cdot (\boldsymbol{X} - \boldsymbol{X_c}),$$

where $\boldsymbol{X_c}$ is defined by $\int_c (\boldsymbol{X} - \boldsymbol{X_c})\,\mathrm{d}X\mathrm{d}Y = \boldsymbol{0}$ and $\phi(\boldsymbol{X_c}) = \phi_c$.

- Calculation of $\boldsymbol{\nabla}\phi_c$ by a least square procedure
- Reconstruction exact for linear fields
- Monotony ensured by slope limiters so that

$$\min_{k\in\mathcal{C}(c)} \phi_k \leq \phi_c(\boldsymbol{X_n}) \leq \max_{k\in\mathcal{C}(c)} \phi_k,$$

where $\mathcal{C}(c)$ is the set of the nearest neighbors of cell c.

- Nodal extrapolated values for the nodal solver
- Explicit time discretization by a 2 steps Runge-Kutta procedure

Numerical results

- Sod shock tube, first and second order calculation for $n_x = 100$ cells

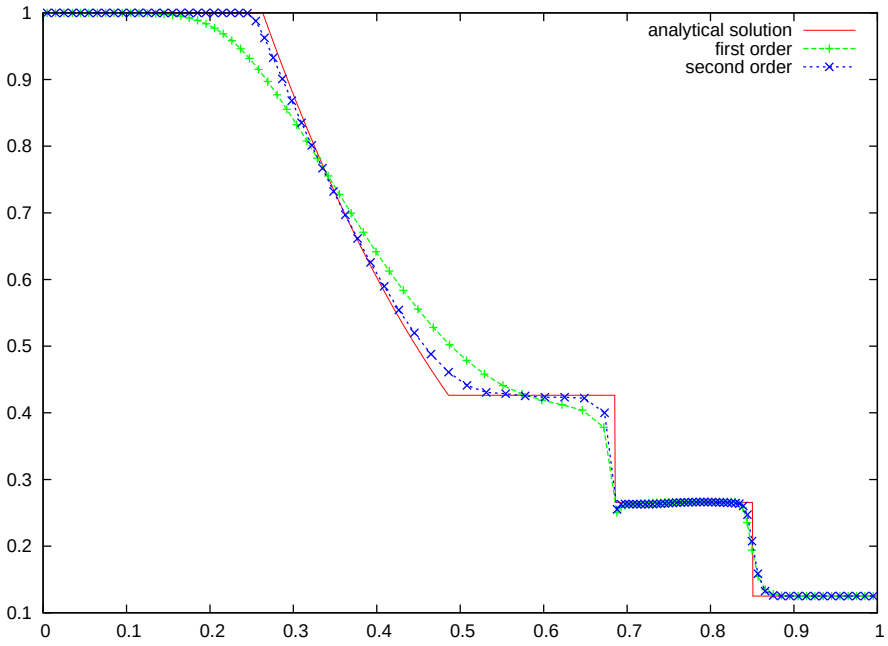

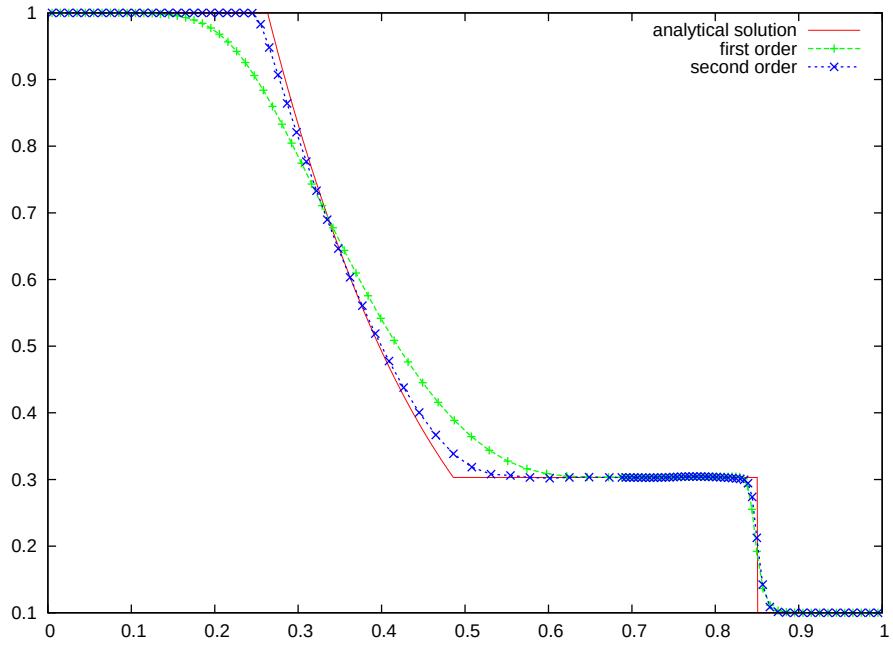

Density and pressure plots at time $t = 0.2$

Numerical results

- Saltzman test case

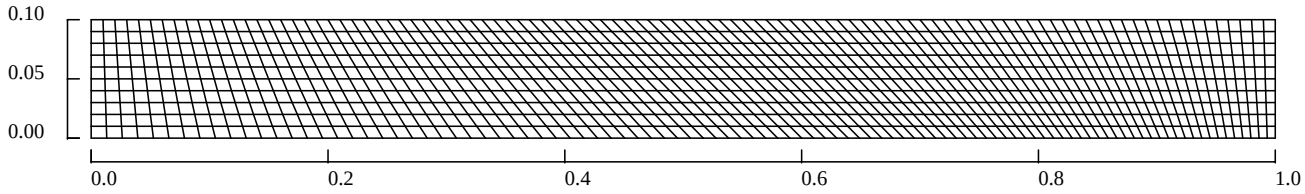

Computational domain $(x, y) \in [0, 1] \times [0, 0.1]$ with $(n_x, n_y) = (100, 10)$ stretched by the map

$$x_{str} = x + (0.1 - y)\sin(x\pi),$$
$$y_{str} = y.$$

Initial conditions: $(\rho^0, P^0, \boldsymbol{V^0}) = (1, 0, 0)$, perfect gas with $(\gamma = 5/3)$.
Inflow velocity $V^\star = -1$ on the left boundary $x = 0$.
Planar strong shock wave with speed $\boldsymbol{D} = \frac{4}{3}\boldsymbol{e_x}$.

Numerical results

- Saltzman test case

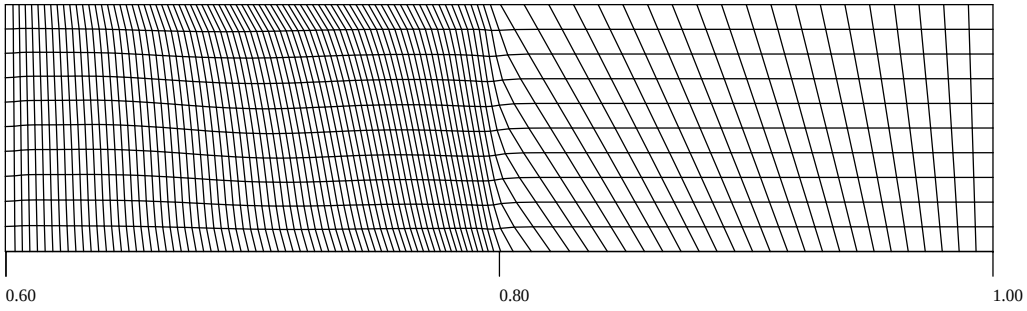

Mesh at $t = 0.6$

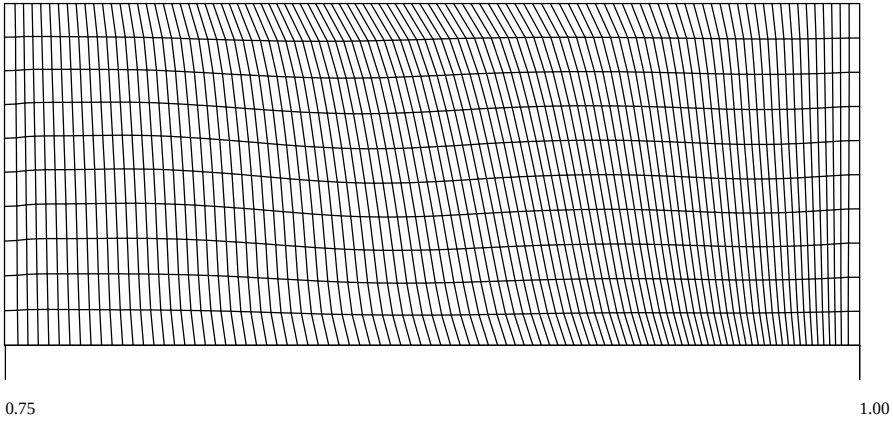

Mesh at $t = 0.75$

Numerical results

- Saltzman test case

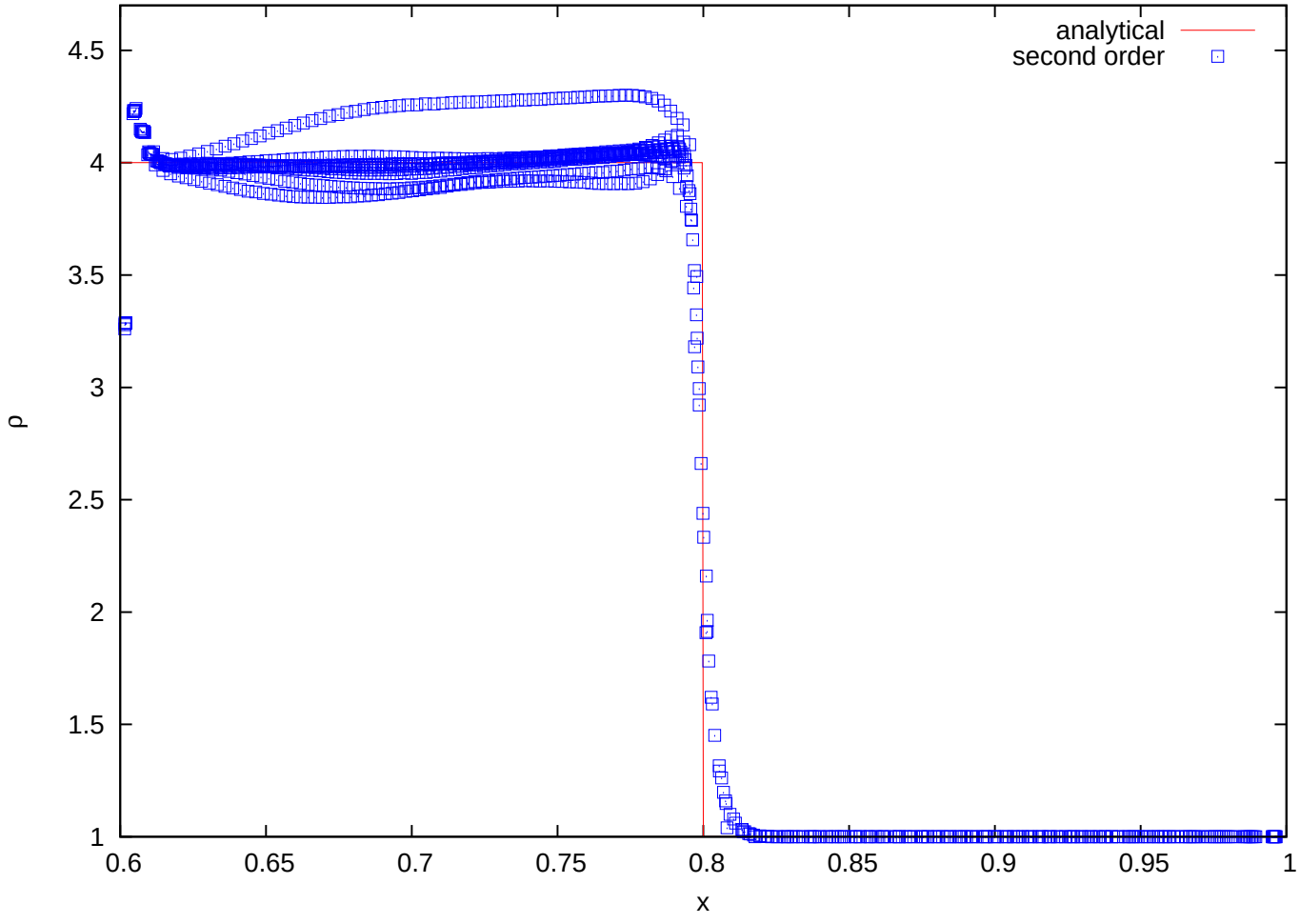

Density in all the cells as function of x at time $t = 0.6$

Numerical results

- Saltzman test case

Mesh at $t = 0.96$

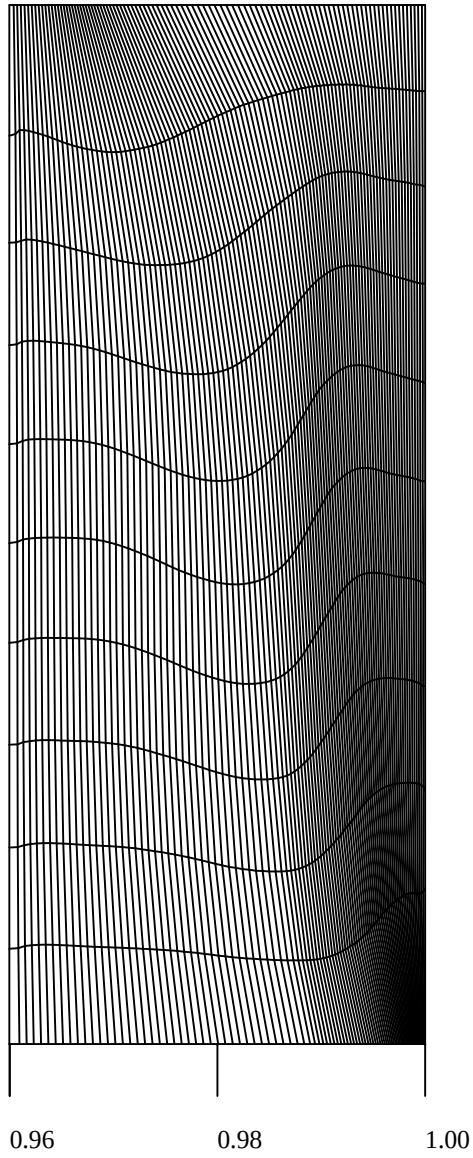

Numerical results

- Noh test case on a 50×50 Cartesian grid

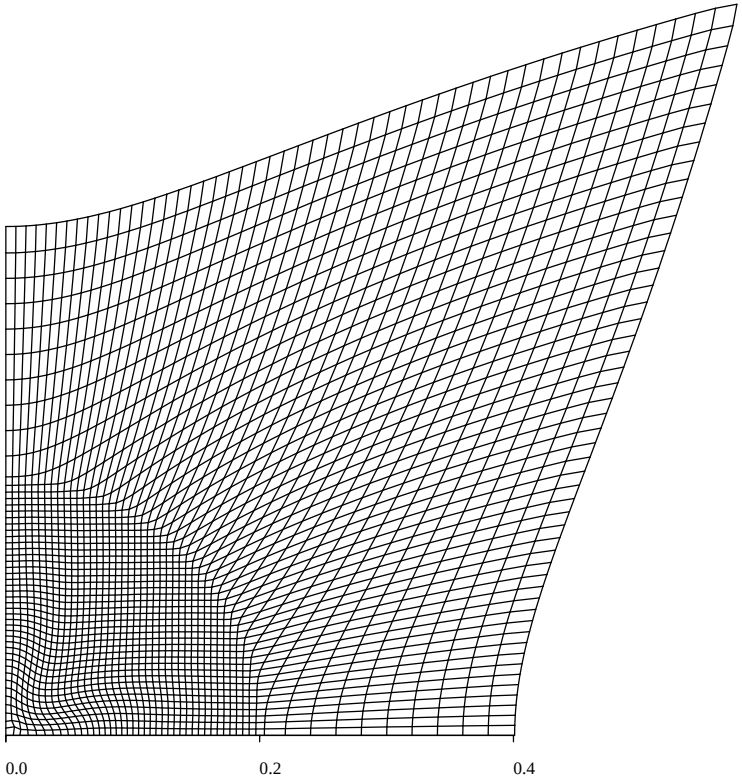

Mesh at $t = 0.6$

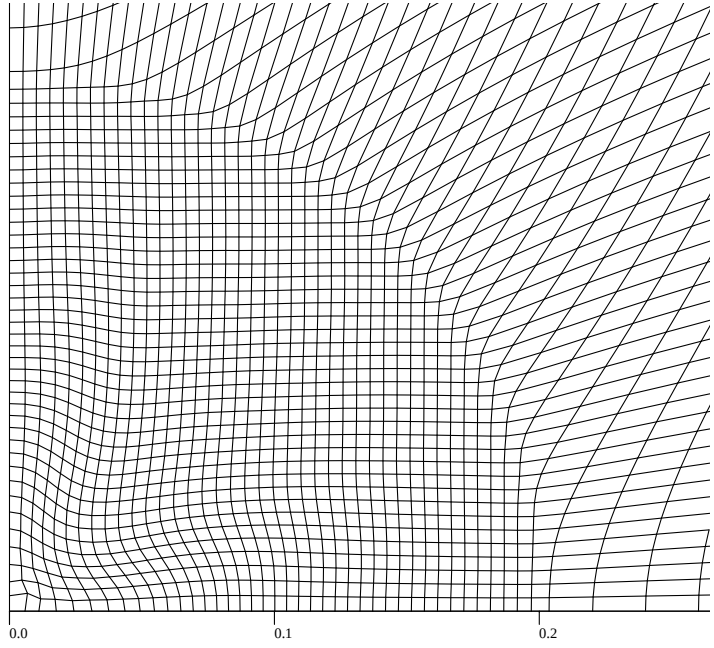

Zoom near the center

Numerical results

- Noh test case on a 50×50 Cartesian grid

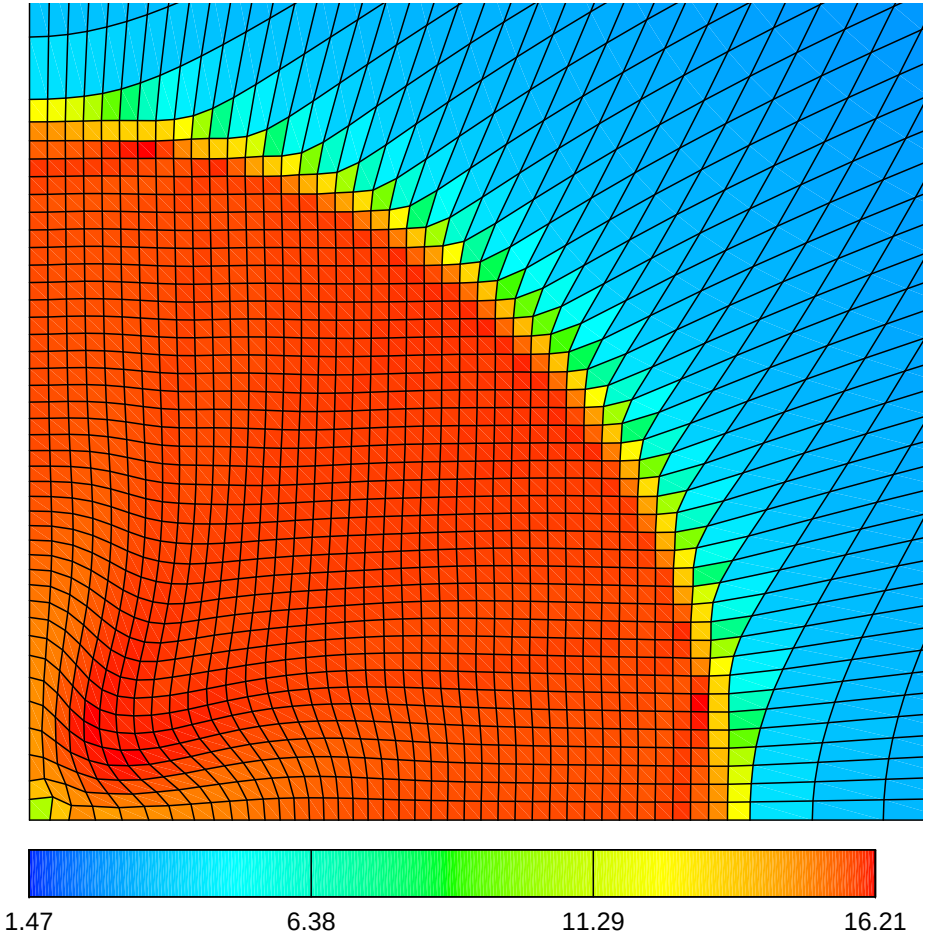

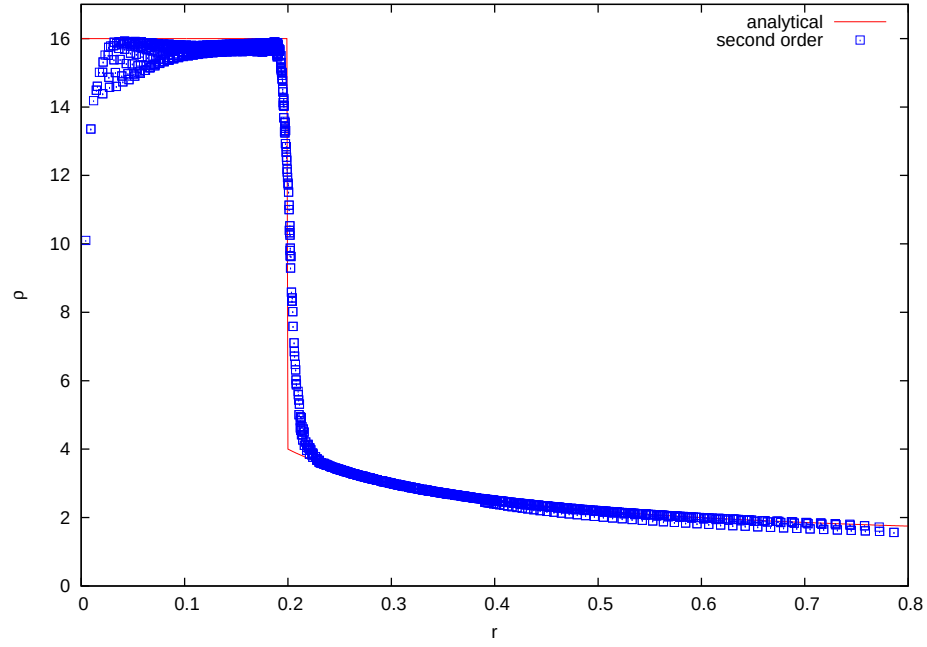

Density map (left) and density in all the cells (right) at $t = 0.6$.

Numerical results

- Sedov test case on a 50×50 Cartesian grid

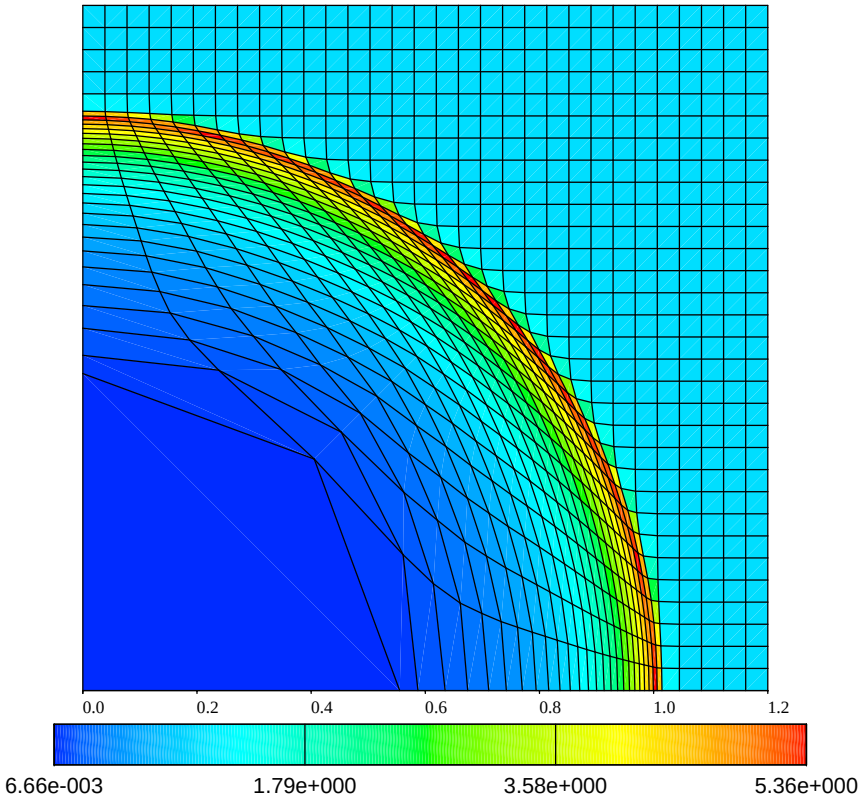

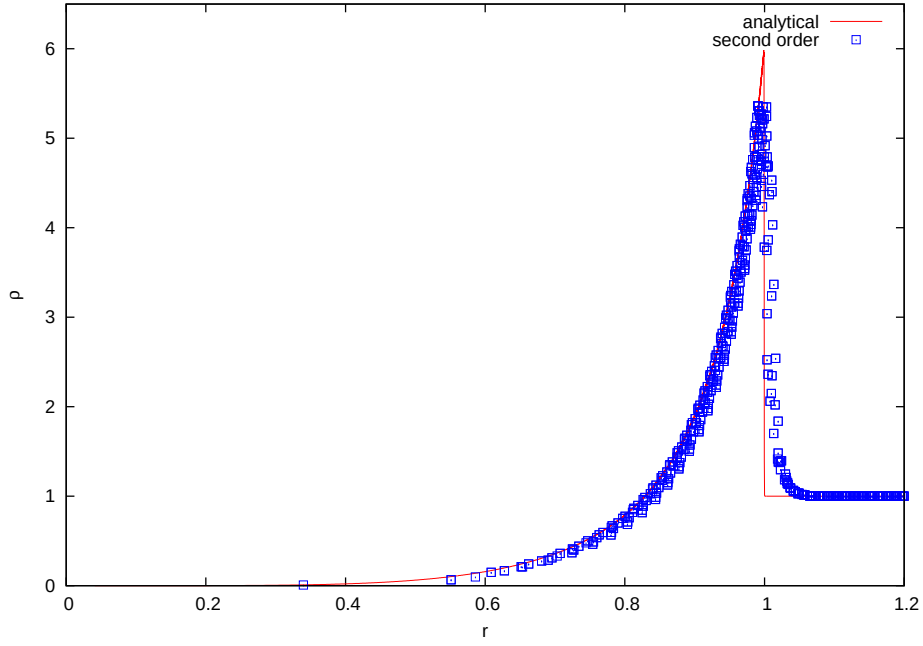

Density map (left) and density in all the cells (right) at $t = 1$.

Ref : R. LOUBÈRE, M.J. SHASHKOV, *A subcell remapping method on staggered polygonal grids for ALE methods*, JCP **209** (2005) 105-138.

Numerical results

- Sedov test case on a polygonal grid

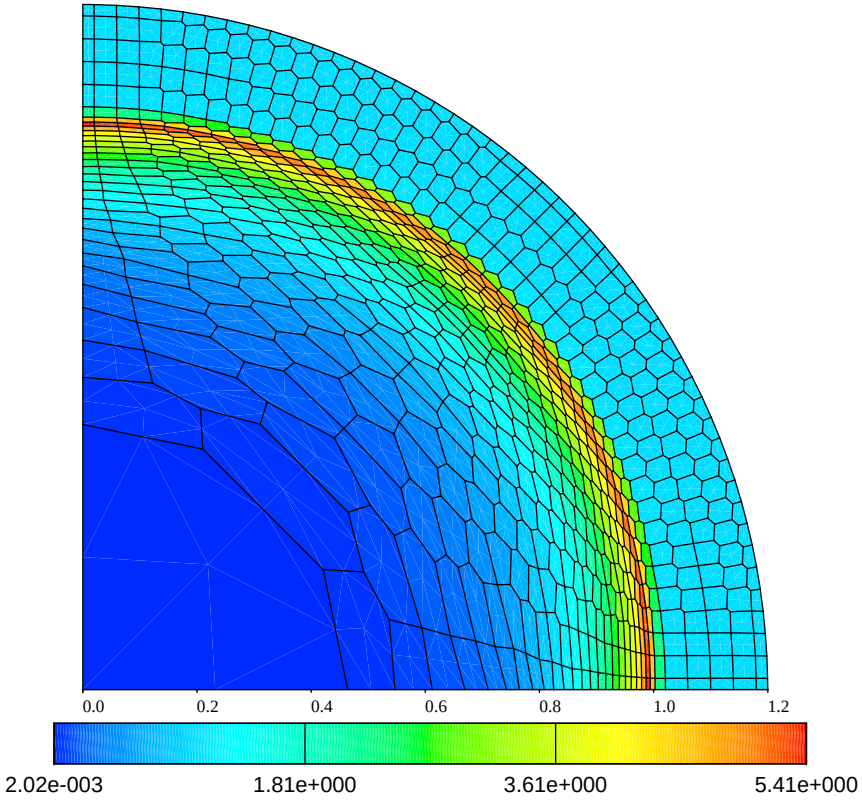

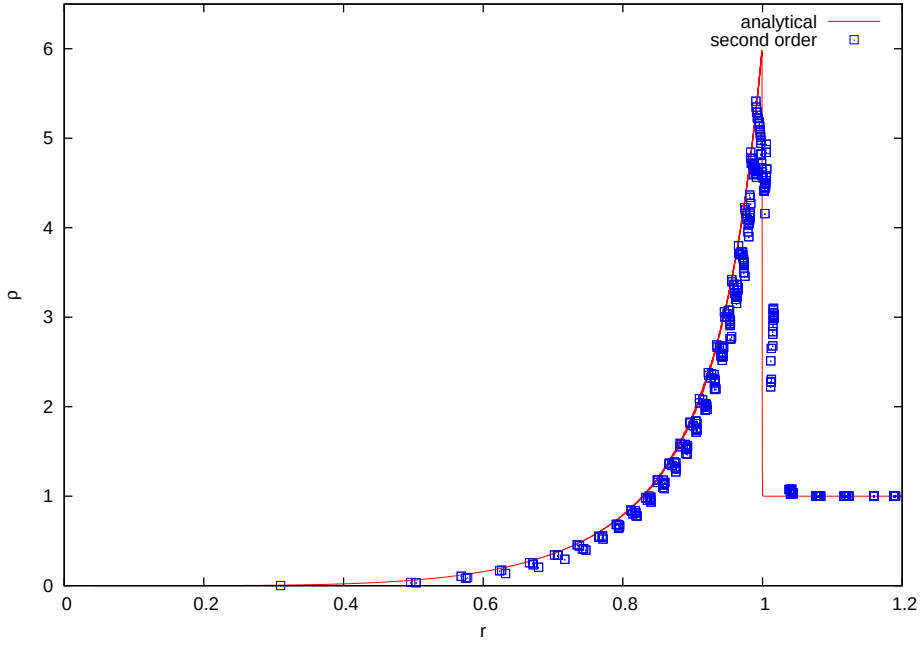

Density map (left) and density in all the cells (right) at $t = 1$.

Numerical results

- Linear phase of Richtmyer-Meshkov instability

Ref : Y. YANG, Q. ZHANG, D. SHARP, *Small amplitude theory of Richtmyer-Meshkov instability*, Phys. Fluids **6**(5), May 1994.

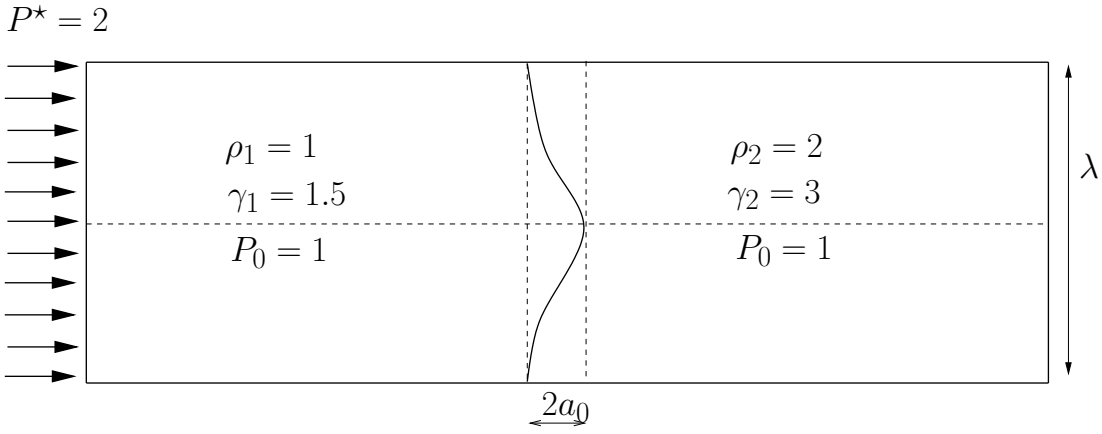

Transmitted shock
Reflected shock
$a_0 = 10^{-4}$

- Perturbation amplitude evaluated with 2D computations

$$a(t) = \left(x_{\text{pert}}(t) - x_{\text{unpert}}(t)\right)/a_0$$

- First and second order calculations
- Comparison with linear theory

Numerical results

- X-t diagram of the flow

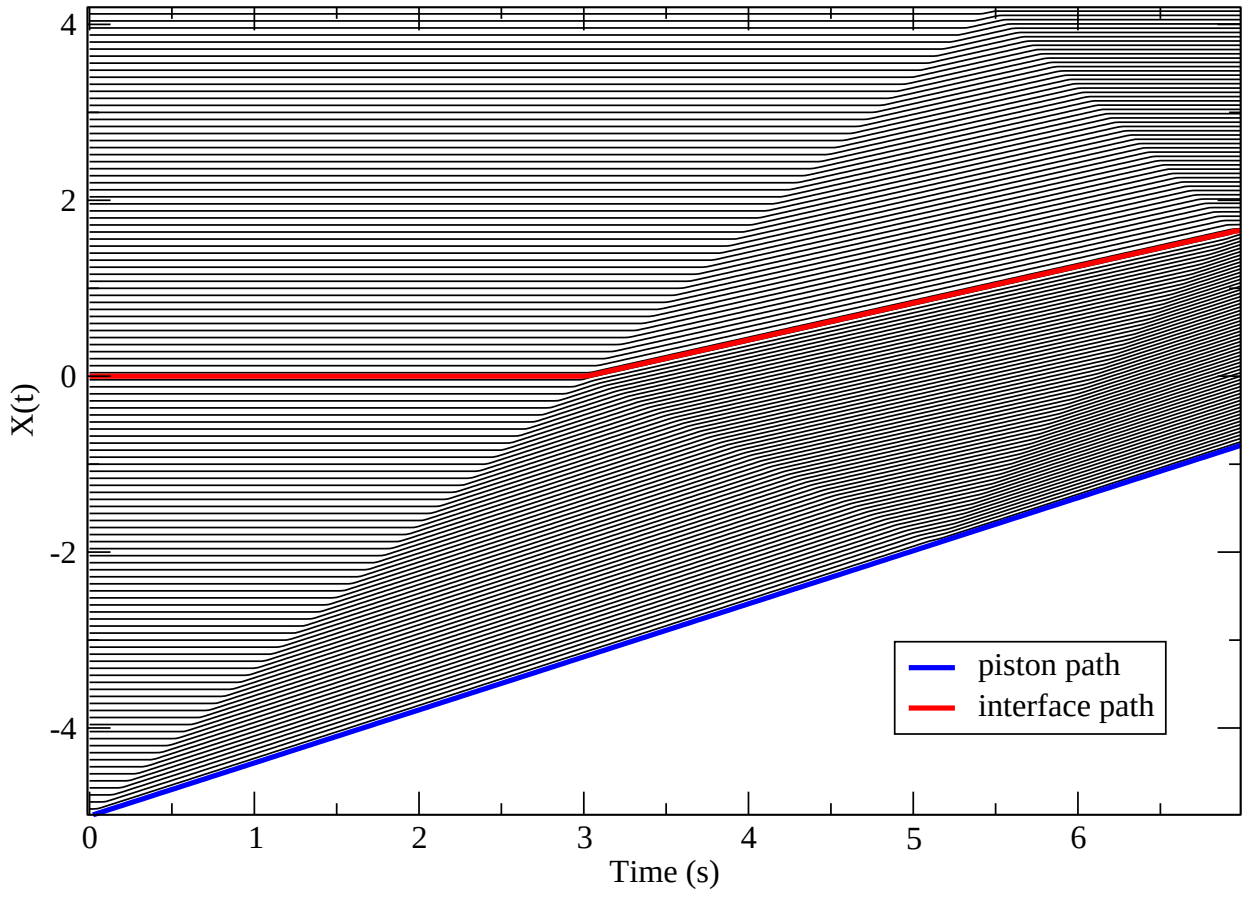

Numerical results

- Perturbation amplitude evolution

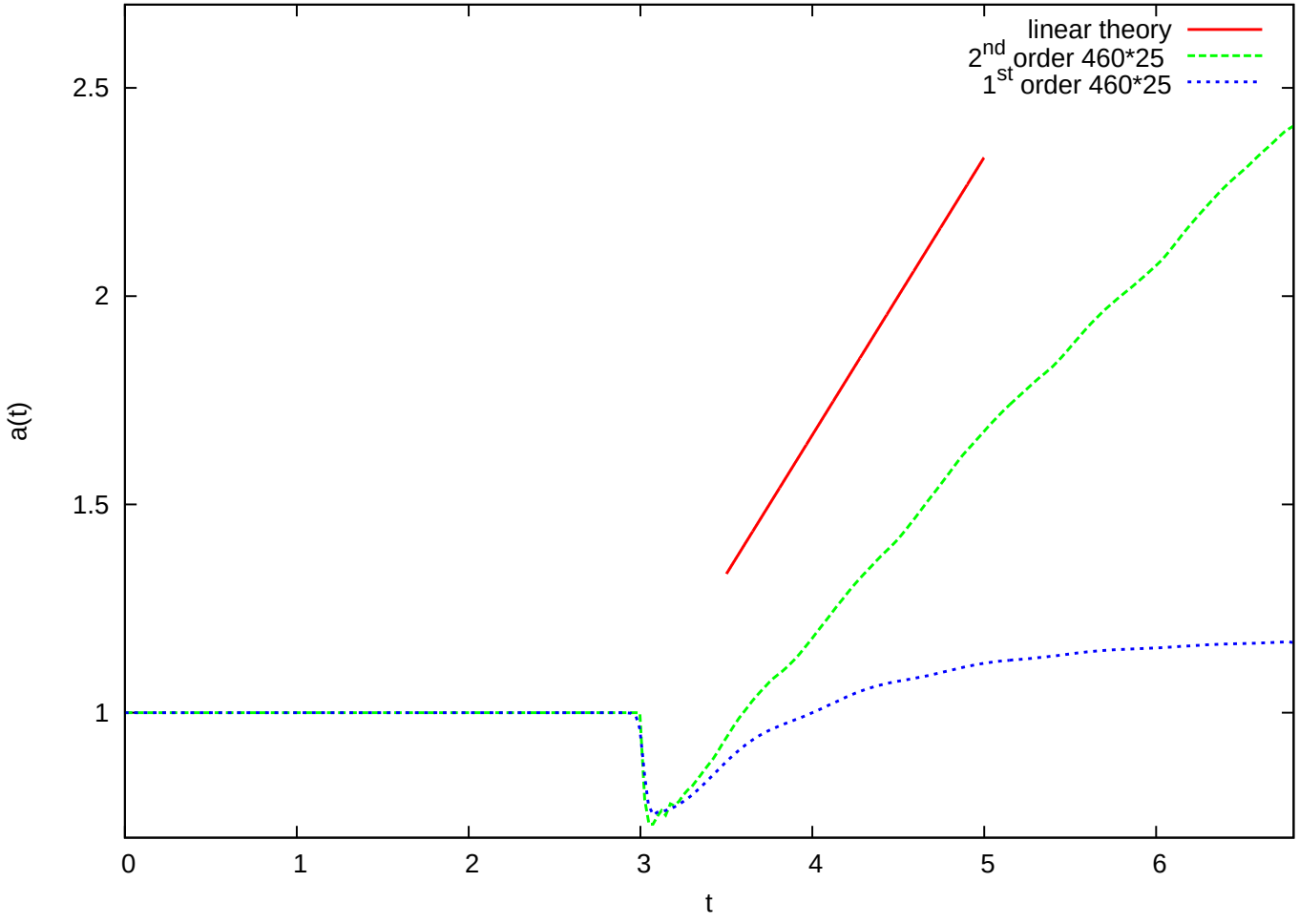

Comparison between first, second order and linear theory

Numerical results

- Rayleigh-Taylor and RM instability for a spherical implosion

Ref : D. YOUNGS, *3D Numerical simulation of turbulent mixing in spherical implosions*, 10^{th} IWPCTM, Paris July 2006.

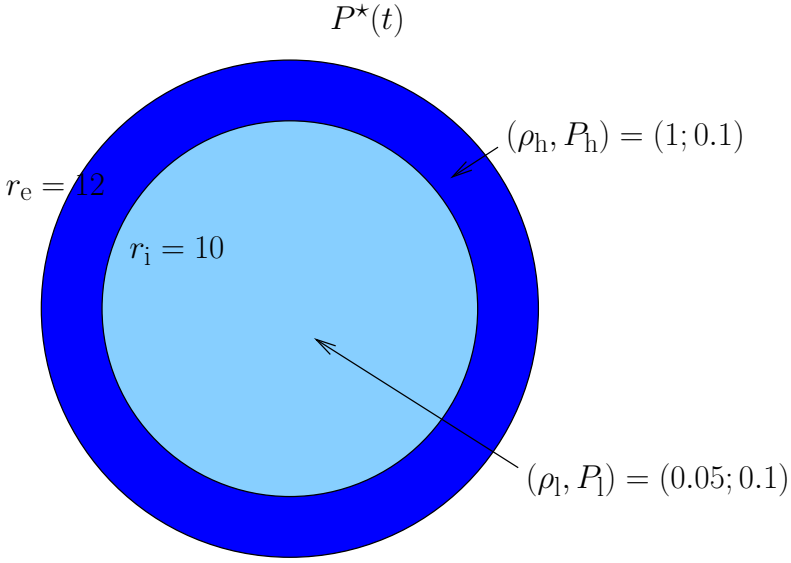

Prescribed pressure

$$P^\star(t) = 10,\ t \in [0; 0.5]$$

$$P^\star(t) = 12 - 4t, t \in [0.5; 3]$$

- Initial perturbation at internal interface with Legendre modes

$$r_\mathrm{i}^\mathrm{pert} = r_\mathrm{i}\left[1 + a_0 P_l(\cos\theta)\right]$$

- We set $a_0 = 10^{-3}$ and $l = 10$

Numerical results

- R-t diagram of the spherical implosion

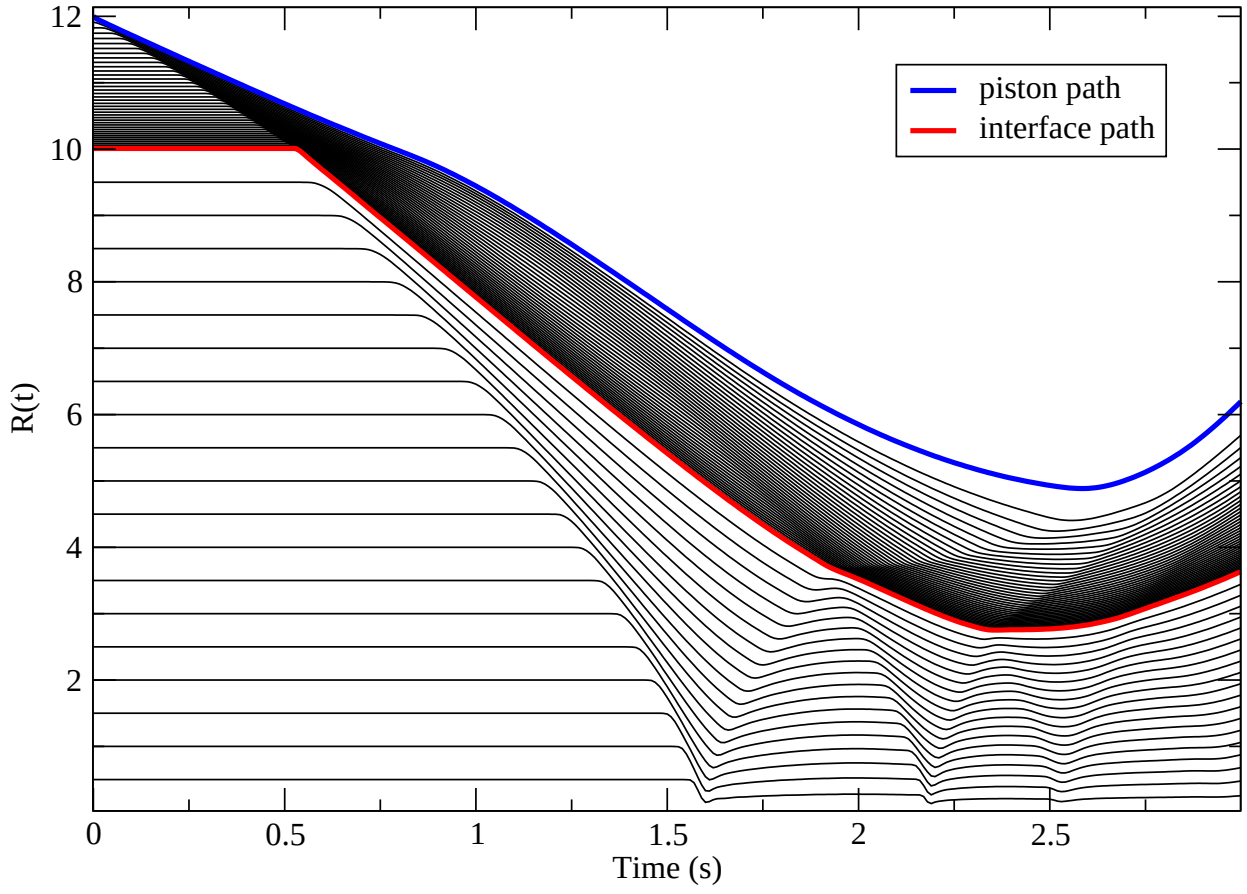

Numerical results

- Development of the RT instability

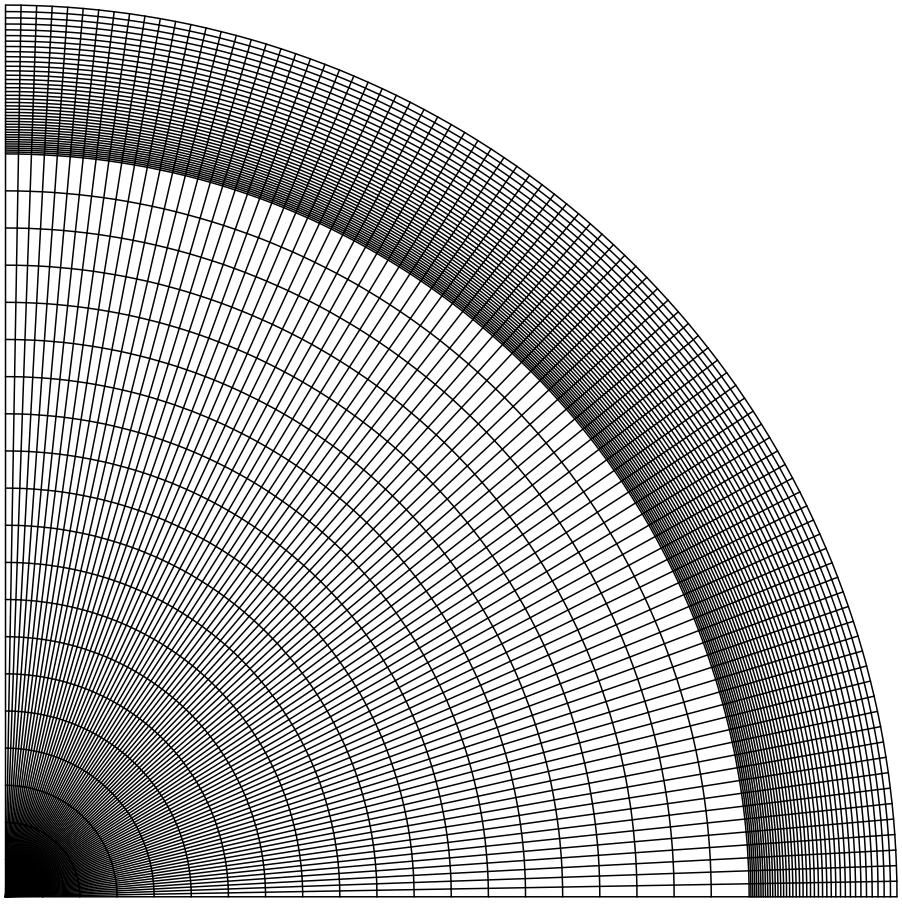

Initial grid

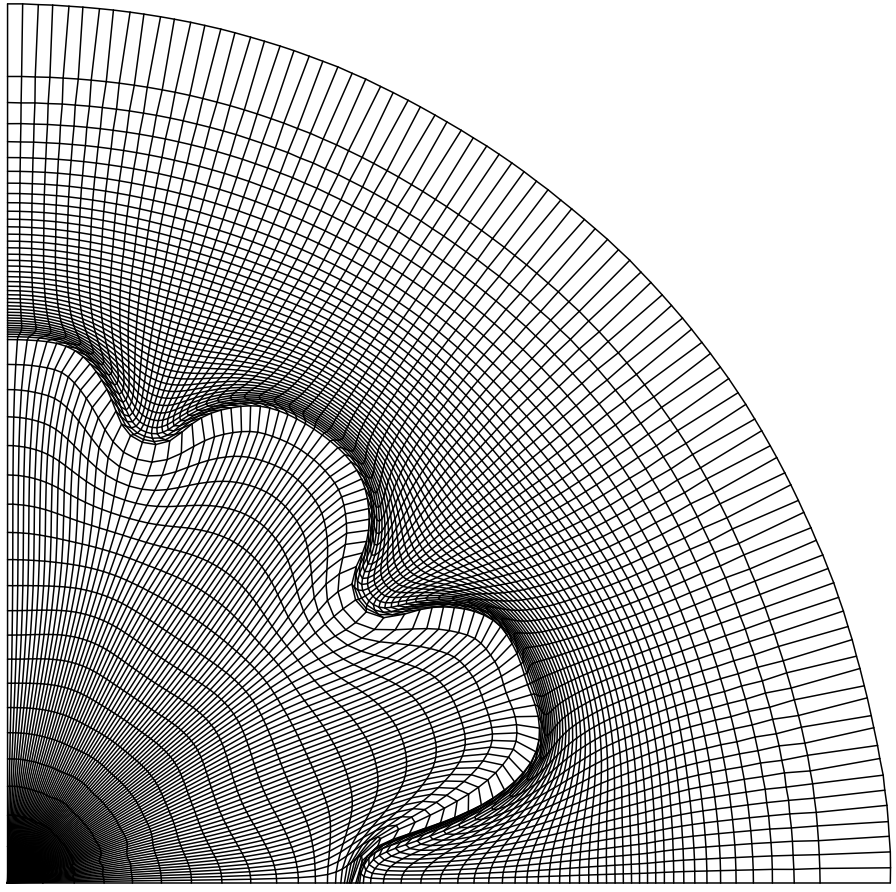

Final grid

Numerical results

- Development of the RT instability

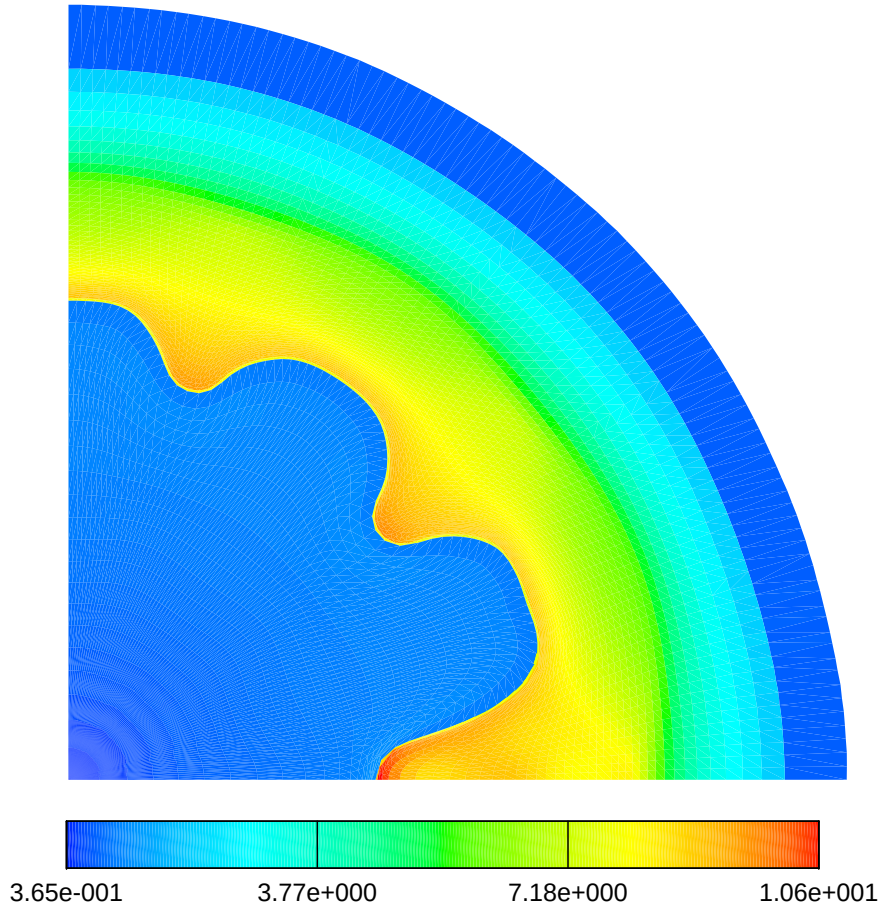

Density map at final time

Experiment design

- Impact of irradiation symmetry on cylinder compression

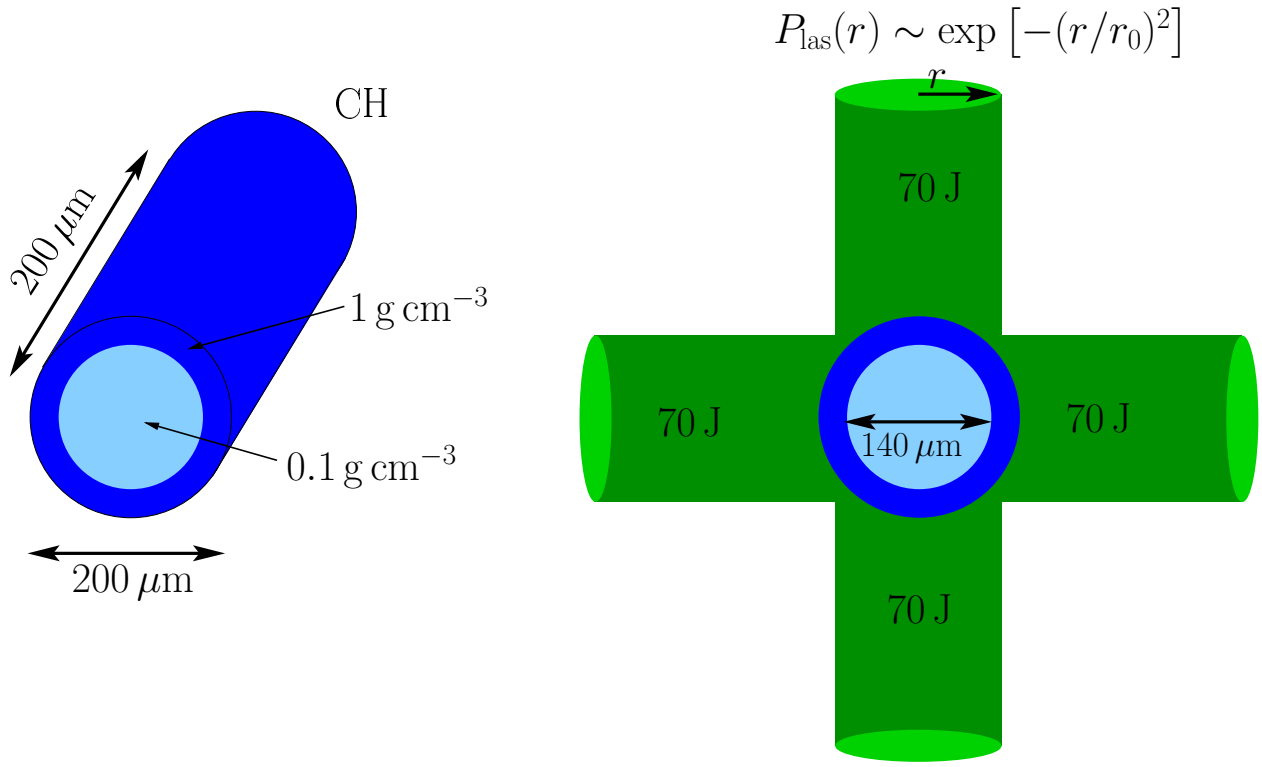

$\lambda_{\mathrm{las}} = 0.53\,\mu\mathrm{m}$, 1 ns square pulse (animation).

Submitted expirement (Vulcan laser facility, Rutherford Appleton Laboratory, 2008, HIPER project).

Experiment design

- Impact of irradiation symmetry on cylinder compression

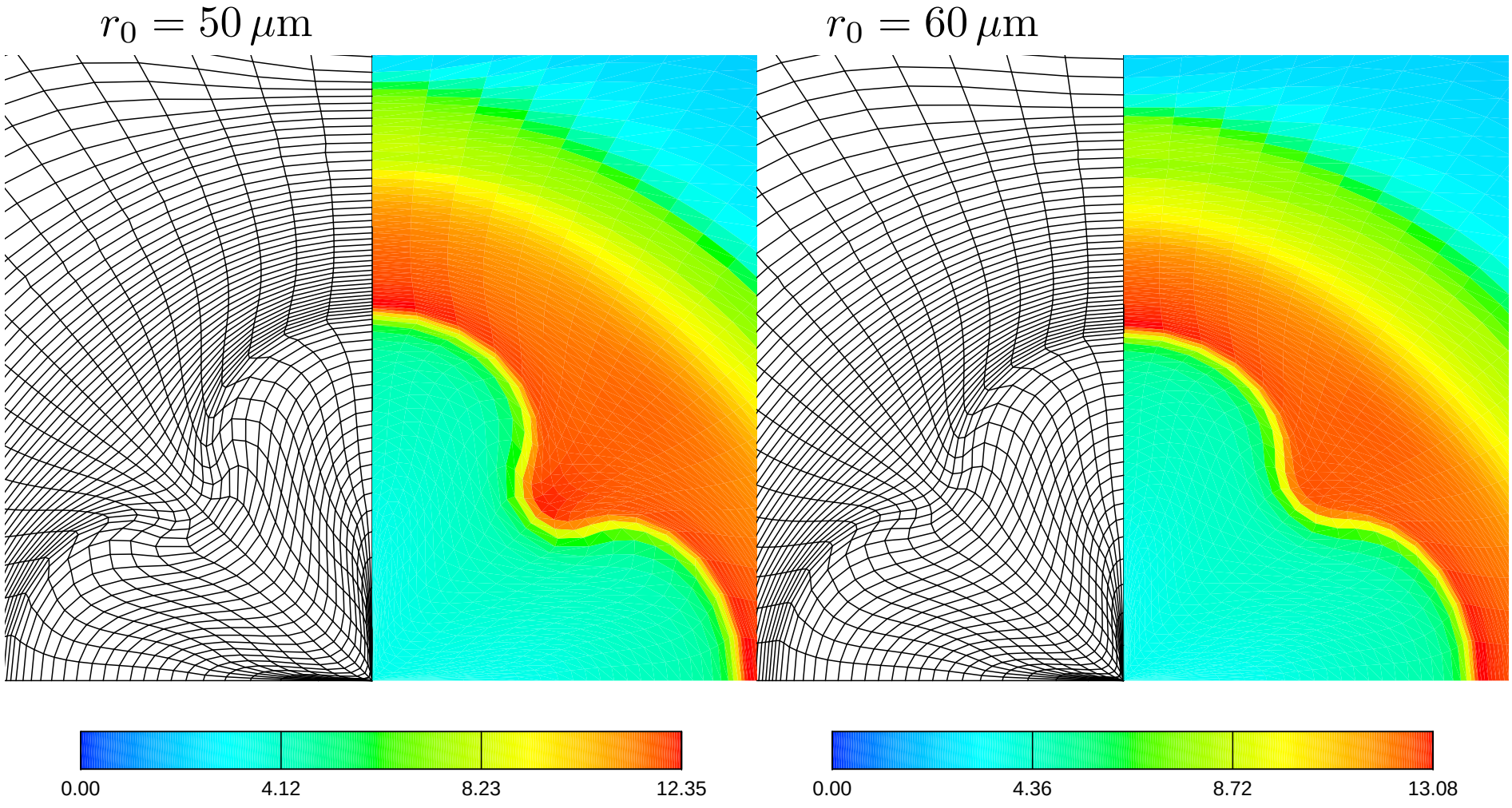

Map density at the stagnation

Experiment design

- Impact of irradiation symmetry on cylinder compression

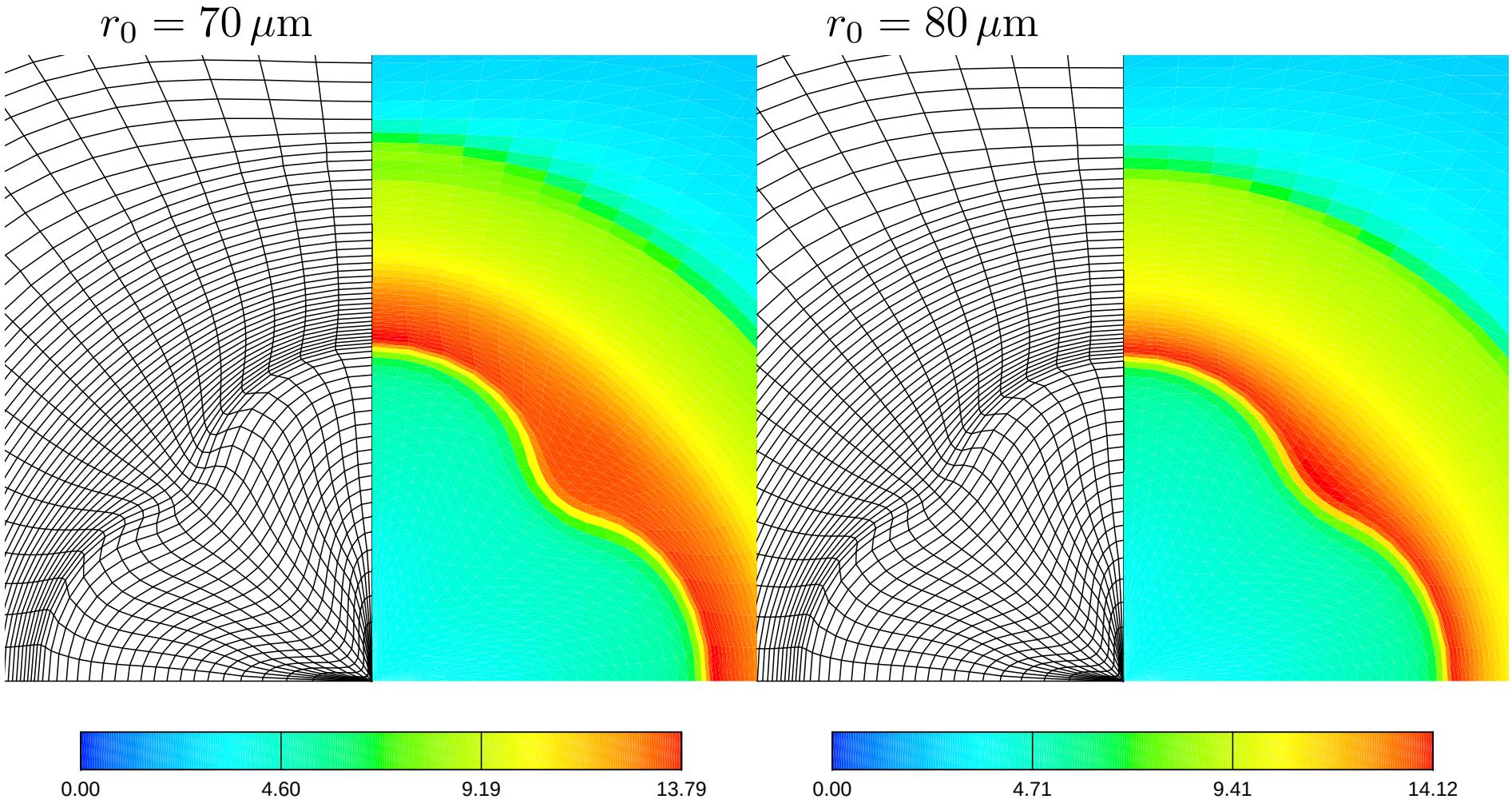

Map density at the stagnation

Experiment restitution

- Characterization of non local heat transport
- Several shots on LIL laser (CEA Bordeaux, December 2005)

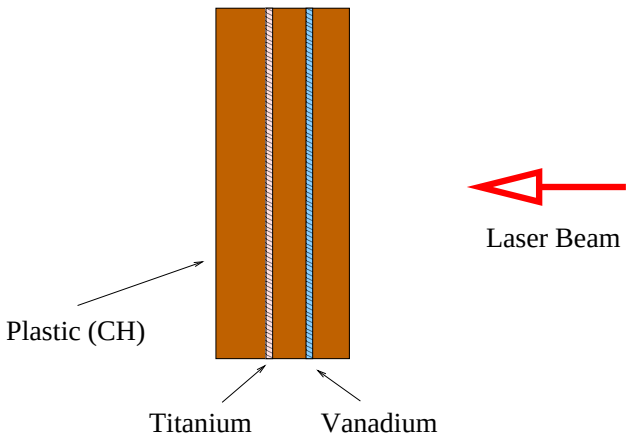

- ◇ Plastic target with Vanadium and Titanium markers of $200\ \mu\mathrm{m}$ thickness
- ◇ Vanadium marker of $0.1\ \mu\mathrm{m}$ thickness at $5\ \mu\mathrm{m}$
- ◇ Titanium marker of $0.1\ \mu\mathrm{m}$ thickness at $15\ \mu\mathrm{m}$
- ◇ Include steady state radiative physics and MHD
- ◇ LIL laser beam : $\lambda = 0.35\ \mu\mathrm{m}$, maximal intensity $1.\ 10^{15}\mathrm{W\ cm}^{-2}$

Ref : G. SCHURTZ ET AL, *Revisiting nonlocal electron-energy transport in Inertial Fusion conditions*, PRL **98**, 2007.

Experiment restitution

Map of electronic temperature

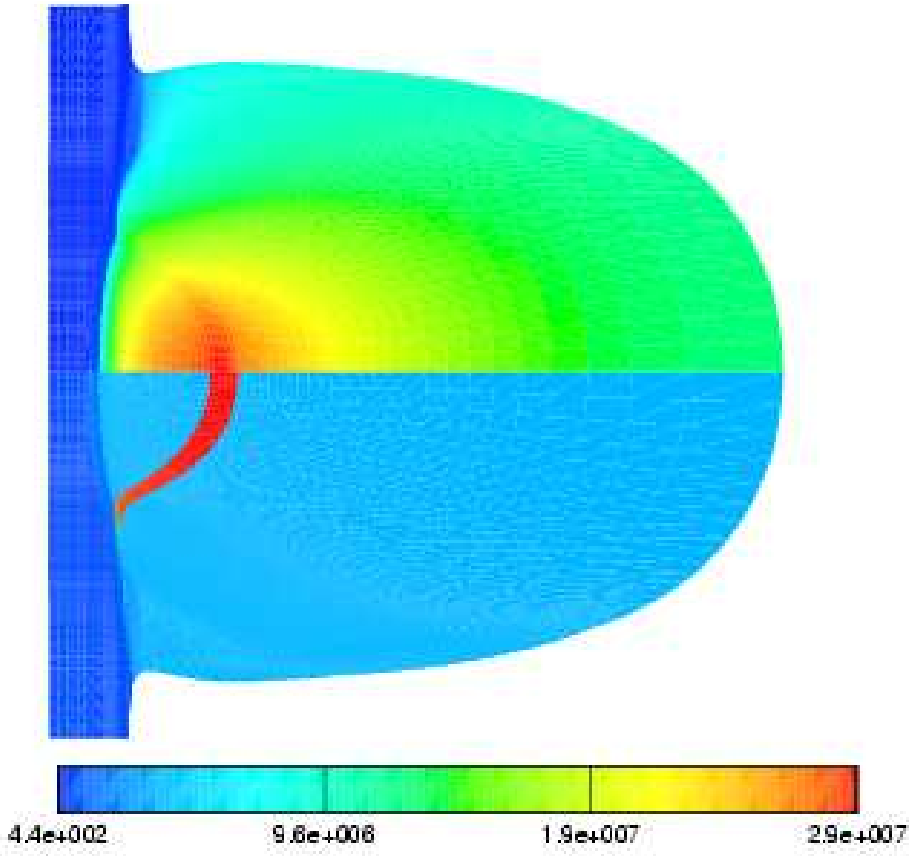

Map of ionization level

Motivations for ALE methodology

- Lagrangian computations can degenarate
- Degenerate typicaly for shear or rotational flows (high velocity impact)
- Can be treated by Arbitrary Lagrangian-Eulerian method

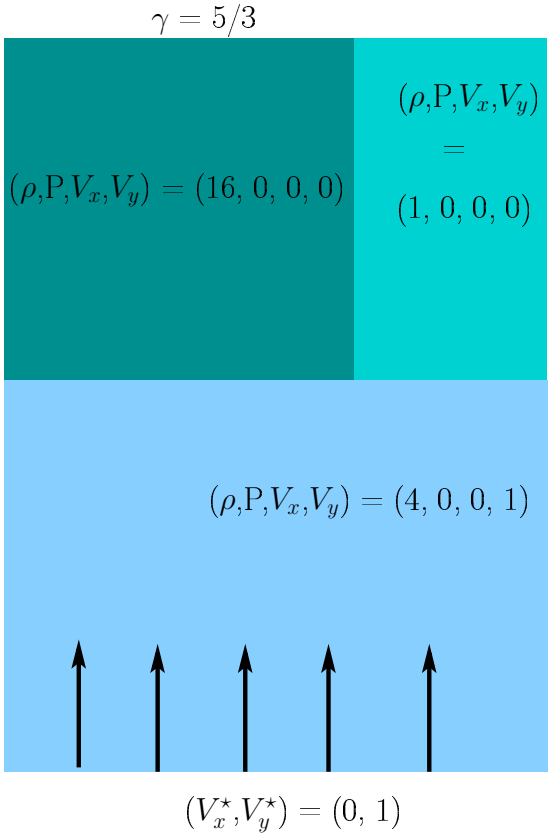

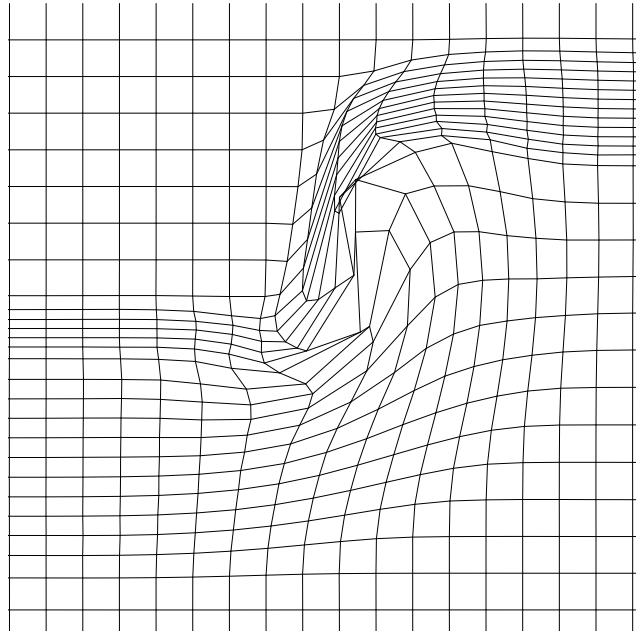

Lagrangian grid, zoom at the corner

ALE methodology

- ALE: combination of Lagrangian and Eulerian methods (Hirt, Amsden, Cook JCP 1974, 1997)
  - Lagrangian computation (several time step)
  - Rezoning : mesh untangling and smoothing
  - Remapping : conservative interpolation of conservative variables from Lagrangian to rezoned mesh
- Remapping allows mass flux between cells
- ALE strategy combines good features of both Lagrangian and Eulerian approaches

Rezoning

- Goal : improvement of unstructured mesh quality
- Minimization of nodally based objective functions (Knupp IJNME **48** 2000)
- Local objective function based on geometric entities associated with the node
- Main issue : how can we incorporate physical criteria in rezoning?

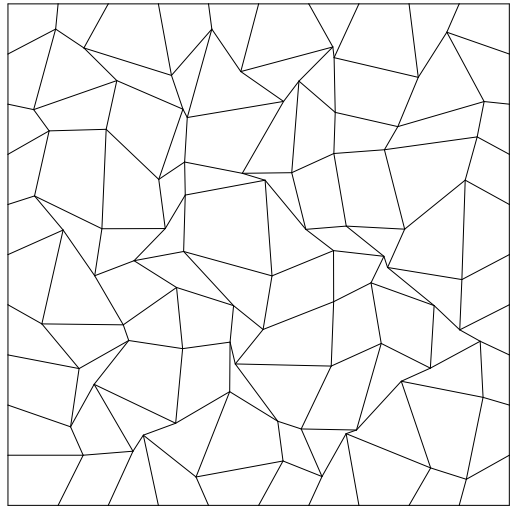

Rezoning

- Nodally based objective function

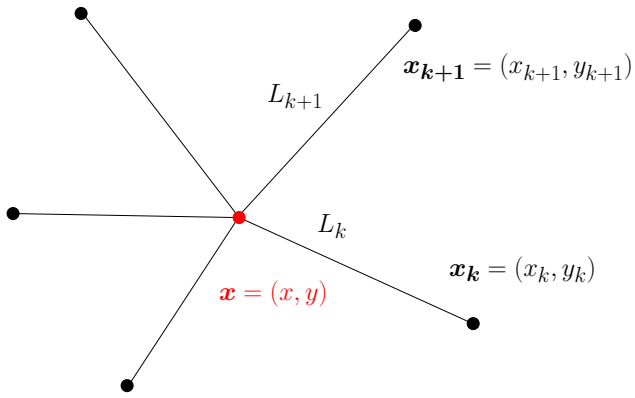

$\boldsymbol{e_k} = \boldsymbol{x_k} - \boldsymbol{x}$, edge vector

$\mathsf{J_k} = [\boldsymbol{e_k}, \boldsymbol{e_{k+1}}]$, Jacobian matrix

Objective function based on *the condition number of the Jacobian matrix*

$$F_s(x,y) = \frac{1}{2} \sum_k \|\mathsf{J_k}^{-1}\| \|\mathsf{J_k}\|,$$

where $\|\|$ is the Frobenius norm. F_s is the discrete analog of the *smoothness functional* proposed by Brackbill (JCP **46**, 1982). It is closely related to the Winslow smoother.

$$F_s(x,y) = \frac{1}{2} \sum_k \frac{L_k^2 + L_{k+1}^2}{|\ \mathsf{J_k}\ |}.$$

Rezoning

- Nodally based objective function

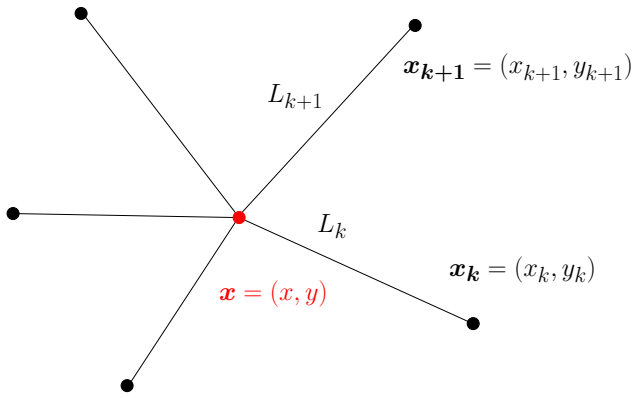

$\boldsymbol{e_k} = \boldsymbol{x_k} - \boldsymbol{x}$, edge vector

$\mathrm{J_k} = [\boldsymbol{e_k}, \boldsymbol{e_{k+1}}]$, Jacobian matrix

In the same framework we derive a weighted orthogonality control functional

$$F_o(x,y) = \frac{1}{2} \sum_k \frac{\left(\boldsymbol{e_k} \cdot \boldsymbol{e_{k+1}}\right)^2}{|\ \mathrm{J_k}\ |^2}.$$

F_o is the discrete analog of the *orthogonality control functional* proposed by Brackbill (JCP **46**, 1982).

Rezoning

- Nodally based objective function

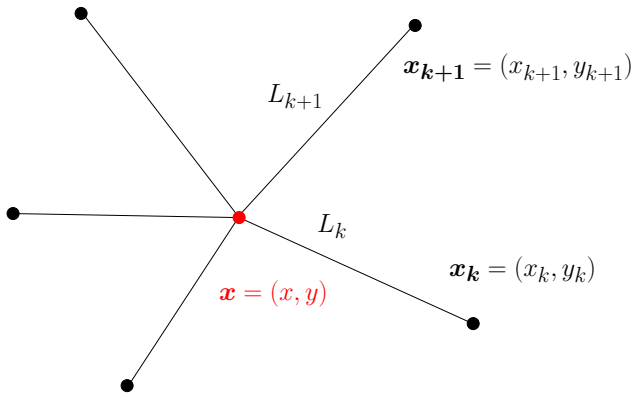

$\boldsymbol{e_k} = \boldsymbol{x_k} - \boldsymbol{x}$, edge vector

$\mathsf{J_k} = [\boldsymbol{e_k}, \boldsymbol{e_{k+1}}]$, Jacobian matrix

We also derive a weighted area control functional

$$F_w(x, y) = \frac{1}{2} \sum_k W_k \mid \mathsf{J_k} \mid^2,$$

W is a weight function resulting in a finer grid where the weight is large.

Contrarily to F_s and F_o, F_w has a physical dimension. Consequently, it is difficult to combine these 3 objective functions.

Rezoning

- Optimization of the global mesh
  - ◇ Construct a local objective function $F(x, y)$ by combining F_s, F_o and F_w
  - ◇ Minimize separately each of the local objective function with a Newton procedure (single step towards the minimum)
  - ◇ Iterate over all the nodes of the mesh
- Treatment of boundary and interface nodes
  - ◇ Boundaries and interfaces are fitted with Bezier curves
  - ◇ Nodes are assigned to move on these Bezier curves
  - ◇ It leads to constrained minimization problem
- Mesh untangling by combination of feasible set method and numerical optimization [Vachal, Garimella, Shashkov (JCP, 2004)].
- Main issue : we need to move only those vertices which are necessary and as little as possible

Remapping

- Conservative interpolation of conservative quantities from the old Lagrangian mesh to the new rezoned mesh
- Piecewise monotonic linear reconstruction over the Lagrangian mesh
- Approximate quadrature over regions swept by edges moving from Lagrangian position to the rezoned position
- Integral over new cells=sum of integrals over swept regions
- Cheaper than exact integration for wich intersections is needed

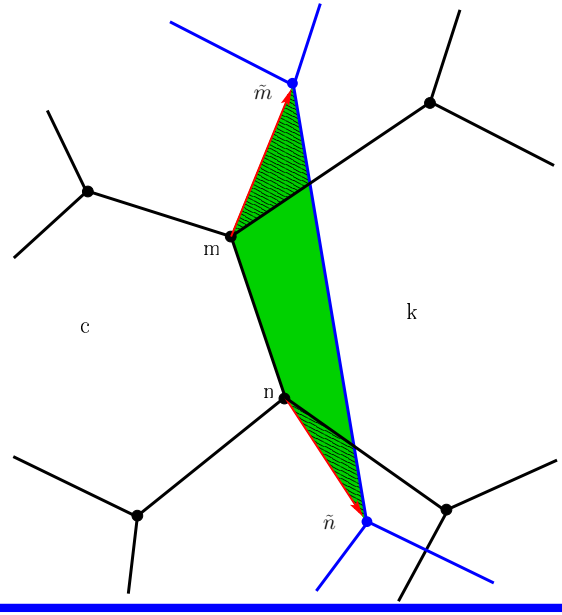

ALE results

- Sedov test case on a 50×50 Cartesian grid

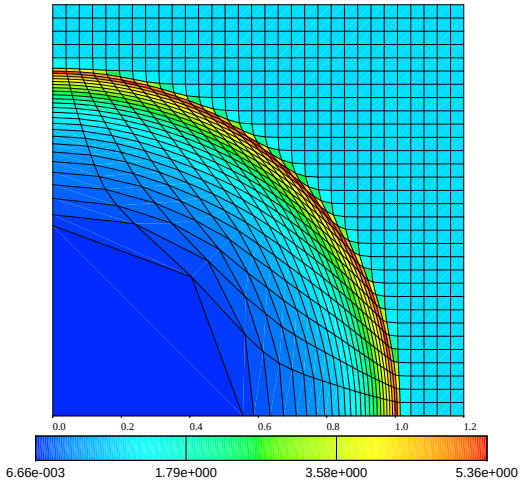

Lagrange

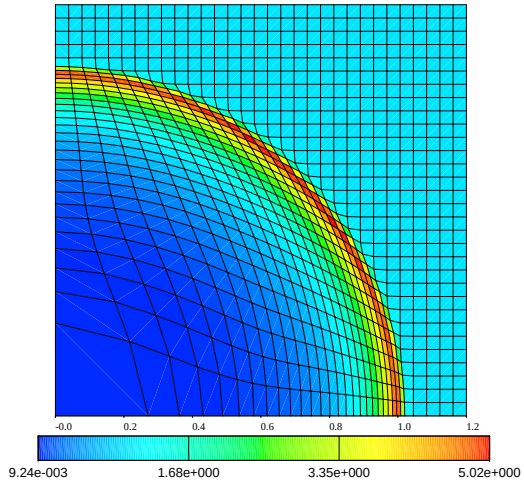

ALE

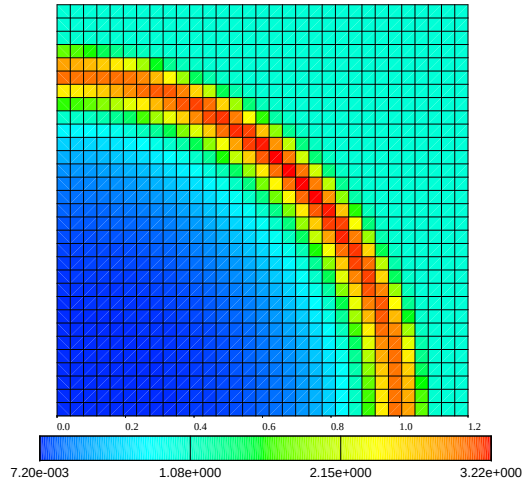

Euler

Density maps at $t = 1$

ALE results

- Sedov test case on a 50×50 Cartesian grid

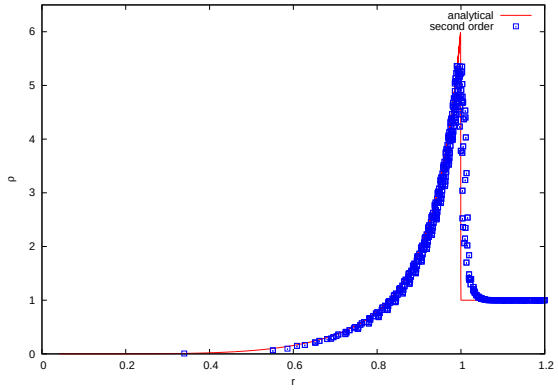

Lagrange

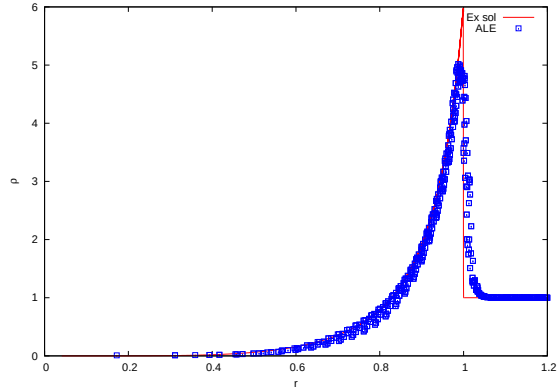

ALE

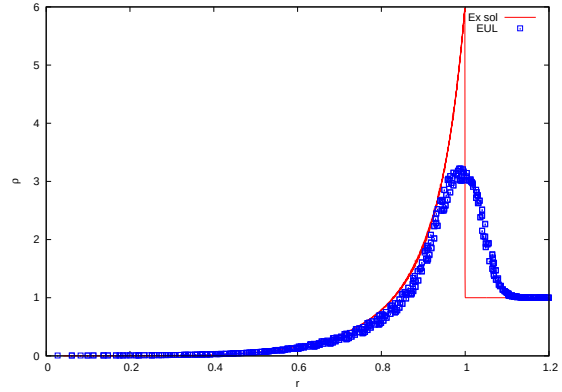

Euler

Density in all the cells versus exact solution at $t = 1$.

ALE results

- Non-linear phase of Richtmyer-Meshkov instability

Ref : C. MÜGLER, L. HALLO ET AL., *Validation of an ALE Godunov Algorithm for Solutions of the Two-Species Navier-Stokes Equations*, AIAA 96-2068, June 1996.

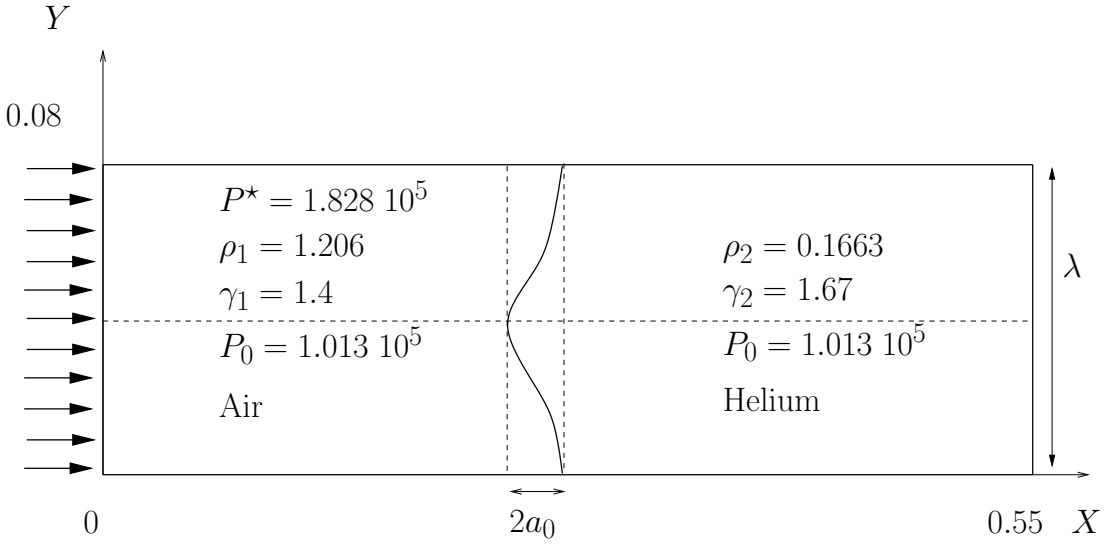

Transmitted shock
Reflected rarefaction wave
$a_0 = 0.32\ 10^{-2}$

- ◇ Initial perturbation $X_{\text{inter}} = 0.4 + a_0 \cos(\frac{2\pi}{\lambda} Y)$
- ◇ ALE second order calculation
- ◇ Mixture assumption isoP, isoT
- ◇ 3 Meshes, cell sizes: $2 \times 2\ mm^2$, $1 \times 1\ mm^2$ and $0.5 \times 0.5\ mm^2$

ALE results

- X-t diagram of the flow

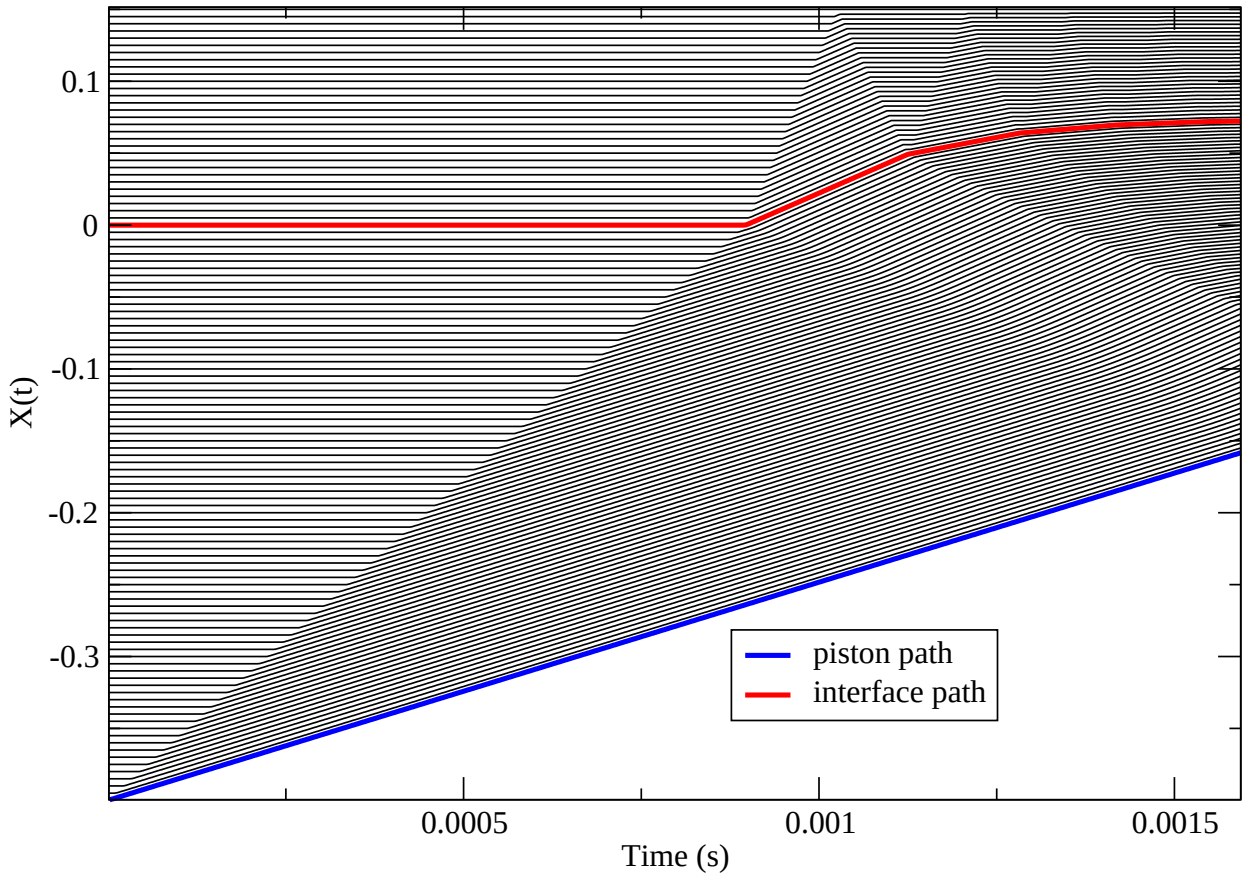

ALE results

- Non-linear phase of Richtmyer-Meshkov instability

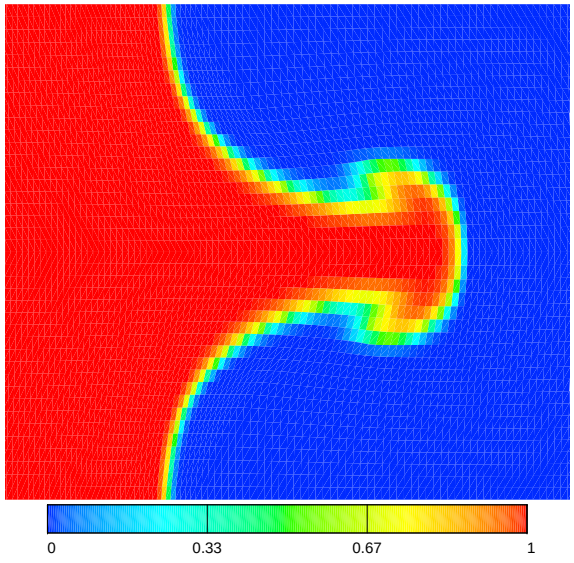

Cell size $2 \times 2\ mm^2$

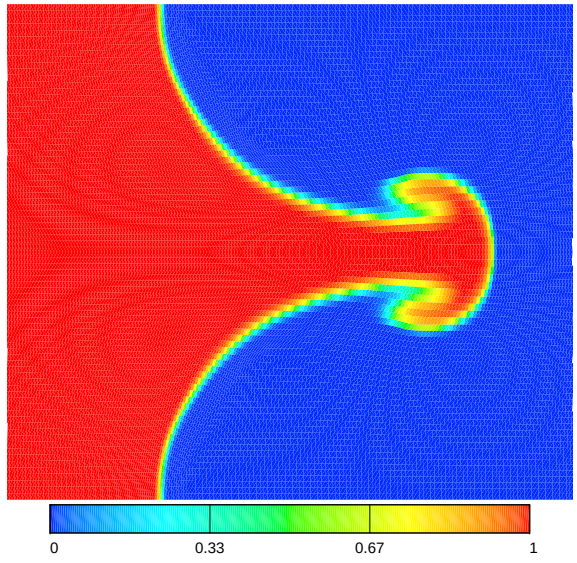

Cell size $1 \times 1\ mm^2$

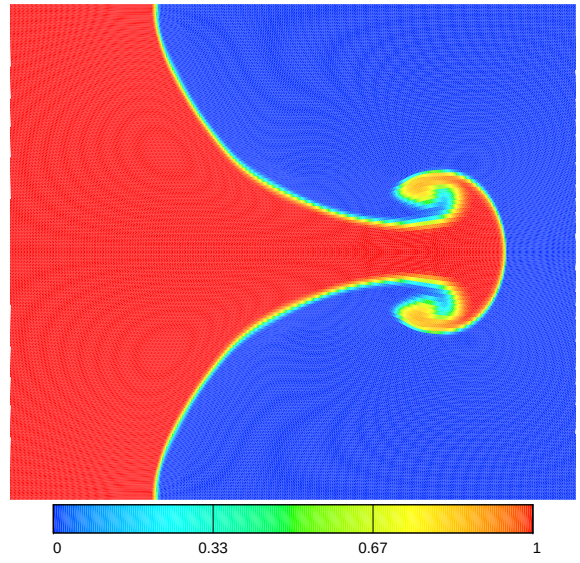

Cell size $0.5 \times 0.5\ mm^2$

Concentration maps at $t = 15.973\ 10^{-4}$ s

ALE results

- High velocity impact test case

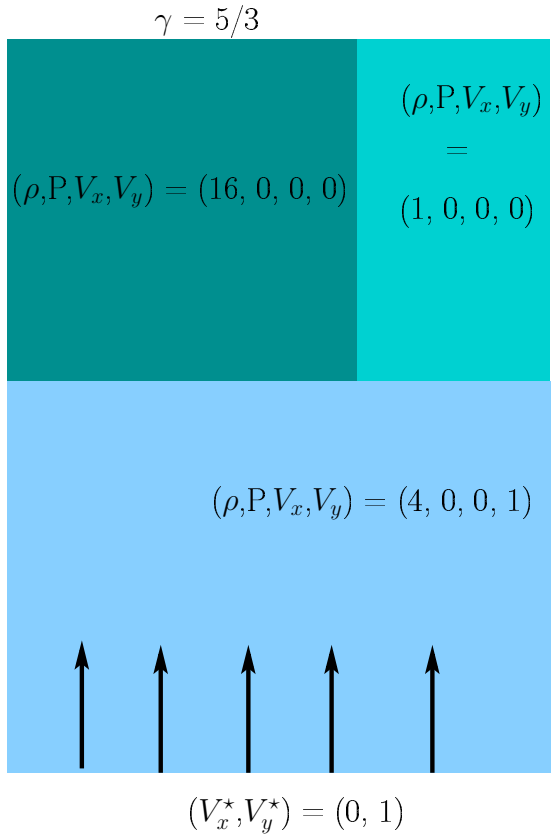

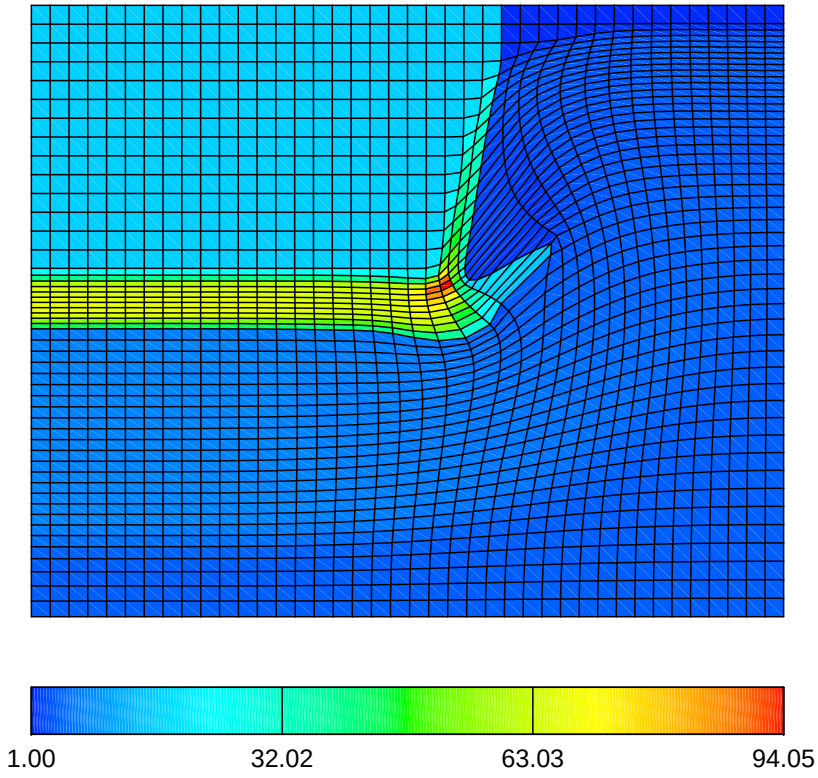

Density map at $t = 0.7$

Conclusions

- An accurate and robust 2D cell-centered second order Lagrangian scheme
- Axisymmetric extension has been achieved
- Coupling with diffusion scheme
- ALE method
- Future works
  - Improvement of rezoning procedure (including physical criteria)
  - Improvement of the nodal solver
  - Three dimensional Lagrangian scheme
  - Interface reconstruction (VOF method)
  - Mixed cells treatment